Gain and Bandwidth Enhancement of Ferrite-Loaded CBS Antenna Using Material Shaping and Positioning

by

Mikal Askarian Amiri

A Thesis Presented in Partial Fulfillment
of the Requirements for the Degree
Master of Science

Approved April 2013 by the
Graduate Supervisory Committee:

Constantine A. Balanis, Chair
James. T. Aberle
Geroge Pan

ARIZONA STATE UNIVERSITY

May 2013

ABSTRACT

Loading a cavity-backed slot (CBS) antenna with ferrite material and applying a biasing static magnetic field can be used to control its resonant frequency. Such a mechanism results in a frequency reconfigurable antenna. However, placing a lossy ferrite material inside the cavity can reduce the gain or negatively impact the impedance bandwidth.

This thesis develops guidelines, based on a non-uniform applied magnetic field and non-uniform magnetic field internal to the ferrite specimen, for the design of ferrite-loaded CBS antennas which enhance their gain and tunable bandwidth by shaping the ferrite specimen and judiciously locating it within the cavity. To achieve these objectives, it is necessary to examine the influence of the shape and relative location of the ferrite material, and also the proximity of the ferrite specimen from the probe on the DC magnetic field and RF electric field distributions inside the cavity. The geometry of the probe and its impacts on figures-of-merit of the antenna is of interest as well.

Two common cavity backed-slot antennas (rectangular and circular cross-section) were designed, and corresponding simulations and measurements were performed and compared. The cavities were mounted on 30 cm $\times$ 30 cm perfect electric conductor (PEC) ground planes and partially loaded with ferrite material. The ferrites were biased with an external magnetic field produced by either an electromagnet or permanent magnets.

Simulations were performed using FEM-based commercial software, Ansys' Maxwell 3D and HFSS. Maxwell 3D is utilized to model the non-uniform DC applied magnetic field and non-uniform magnetic field internal to the ferrite specimen; HFSS however, is used to simulate and obtain the RF characteristics of the antenna. To

validate the simulations they were compared with measurements performed in ASU's EM Anechoic Chamber.

After many examinations using simulations and measurements, some optimal designs guidelines with respect to the gain, return loss and tunable impedance bandwidth, were obtained and recommended for ferrite-loaded CBS antennas.

ACKNOWLEDGEMENTS

Special thanks to my advisor Professor Constantine A. Balanis for his guidance, valuable advice and financial support. My sincere appreciation is extended to the other members of the committee Dr. George Pan and Dr. James T. Aberle for their suggestion and evaluation of the content of this thesis. Special thanks to Craig R. Birtcher for performing measurements to support numerical predictions presented in this thesis. I also thank Victor Kononov and Ahmet C. Durgun who I frequently benefited from their knowledge.

I would also like to express sincere appreciation to the Advanced Helicopter Electromagnetics (AHE) program and the U.S. Air-Force AFRL/RYDX (Electronics Exploration Branch) for their financial support of this research.

This thesis would not be possible without the support and encouragement from my father Reza Askarian Amiri, my mother Mahin Afarin, and my dear sister Camellia Askarian Amiri. No words can express how grateful I am for your love and how very much I appreciate you. This thesis is dedicated to them.

TABLE OF CONTENTS

CHAPTER Page

LIST OF FIGURES

Figure Page

Figure Page

Chapter 1

Introduction

Using ferrite material in an antenna design introduces some interesting features which are mainly due to the of ferrite's nonlinear nature. Since the permeability of a ferrite material depends on its internal magnetic field distribution, its electrical dimension varies when the intensity of applied magnetic field changes. This is the most interesting characteristic of ferrites which impacts the performance of an antenna. Two examples are presented here to illustrate how ferrites influence an antenna's performance:

- Consider an aperture antenna whose maximum radiation direction is normal to the aperture. Placing a slab of ferrite material at the aperture causes the main beam to deviate from its original direction. Now, if the applied magnetic field changes (direction or magnitude), the deviation of the main beam will be influenced due to the change of aperture effective electric dime4 dimensions.

- Placing a ferrite material inside a cavity provides an interesting mechanism to tune its resonant frequency. When an external static magnetic field is applied to the ferrite-loaded cavity, the permeability of the ferrite sample varies due to a change of the internal magnetic field within the ferrite material. Variation of the ferrite permeability results in updated cavity electrical dimensions, which impacts its resonant frequency. Although the bandwidth of a cavity backed-slot antenna is generally narrow, using the ferrite material may broaden its tunable bandwidth. It should be noted that the instantaneous bandwidth of the antenna at each resonant frequency is still narrow, but using ferrite material leads to a wider bandwidth over the tunable range of the resonant frequency.

The second example demonstrates how ferrite material improves some of the operational characteristics of the antenna, such as bandwidth. However, antenna engineers face many challenges in analysing the behaviour and impacts of these nonlinear materials when they are used in antennas. Some of these challenges are:

- Accurate modeling of the magnetic field distribution within the ferrite is of great importance. Obtaining the radiation characteristics of the antenna based on an inaccurate model may lead to unacceptable results.
- Ferrites are lossy materials. Placing a slab of ferrite inside the cavity backed-slot antenna generally results in the reduction of gain.
- When the cavity is loaded with ferrite material, its RF electric field distribution changes. This may cause changes in the input impedance and return loss of the antenna.

There were previous investigations of ferrite loaded CBS antennas [1]-[4].

In [2], the input impedance was obtained assuming that the ferrite sample was biased uniformly. In this approach, both of the applied and demagnetizing fields were assumed to be uniform. Consequently the internal magnetic field would be uniform, i.e., the same direction and constant magnitude at every point inside the ferrite. The magnitude of the uniform internal field was obtained by averaging of the non-uniform magnetic field at different points of the ferrite material. Although the results presented in [2] are in a good agreement with measurements, it was shown later that such an assumption may lead to inaccurate results when the non-uniformity is more severe.

The method presented in [3] was an attempt to determine the non-uniform applied magnetic field within the ferrite specimen. Because of the non-linear mag-

netostatic approach used to obtain the internal magnetic field in [3], the results are more accurate than those of [2]; however, the assumption of uniform applied magnetic field causes the solution of the internal magnetic field to be partially accurate.

In [4], some guidelines for the design of a CBS antenna with higher gain and lower resonant frequency were suggested which were mainly based on experiment.

In [1], the emphasis was on the modeling of the non-uniform applied magnetic field and non-uniform magnetic field within the ferrite specimen. It was demonstrated that assuming a uniform magnetic field does not always lead to an acceptable approximate solution. To obtain an accurate result, the non-uniformity of the applied magnetic field must be taken into account.

The major drawbacks of the ferrite configurations reported in previous studies are low gain and poor impedance match. Therefore, the main objective of this thesis is to develop design guidelines to enhance the gain, tunable bandwidth and impedance match of the CBS antenna by shaping the geometry of the ferrite sample and to judiciously place it within the cavity. The numerical model utilized in this thesis is based on a non-uniform applied magnetic field and non-uniform magnetic field within the ferrite sample reported in [3].

The rest of the thesis is organized as follows. A brief theory of cavity backed-slot antennas and ferrites is presented in Chapter 2. Chapter 3 mainly concentrates on the geometry and modeling of the antenna, ferrite material, electromagnet and permanent magnets with Ansys HFSS and Maxwell 3D. Chapter 4 illustrates the design procedure of an efficient CBS antenna. Different configurations of ferrite material are suggested. Simulations are performed and their results are presented. The RF electric field distribution inside the cavity is observed, and attempts are made to find reasons for the poor performance of the previously reported designs and so-

lutions to overcome their drawbacks. To validate the models and simulated results, measurements were conducted in the ASU EM Anechoic Chamber (EMAC) and their results are compared. In Chapter 5, design guidelines and conclusions are discussed, and they are followed by recommendations for future work.

Chapter 2

Theory

2.1 Introduction

In this chapter a brief theory of the cavity-backed slot antenna is presented. It is known that if a cavity is open on one side, electromagnetic energy will escape and can be radiated through the aperture. Therefore, to understand the performance of CBS antennas, it is necessary to review the theory of cavity resonators. The principles of cavity resonators, such as their resonant frequency and the mechanism of energy storing and dissipation, is briefly discussed in this chapter.

The majority of this thesis is focused on ferrite materials with which the CBS antennas are loaded. Since ferrite materials are nonlinear and they are subjected to DC magnetic field, some preliminary background concerning their behaviour is presented. The permeability tensor for three specific directions of the magnetic field is derived and eventually its general form for an arbitrary direction of magnetic field is presented.

2.2 Cavity Resonators

The geometry of a rectangular and circular cavity is illustrated in Figs. 2.1 and 2.2 respectively. Solving the wave equation inside the cavity and applying the boundary conditions show that the modes excited in a cavity are of standing wave form. Therefore, electric and magnetic energy is stored within the cavity. However, some of the energy is dissipated in the cavity walls, since they are not perfect conductors. Coupling to the cavity can be done by a probe.

2.2.1 Rectangular Cavity

A rectangular cavity can be constructed from a section of a rectangular waveguide which is closed at both ends. To obtain the resonant frequency, the wave equation

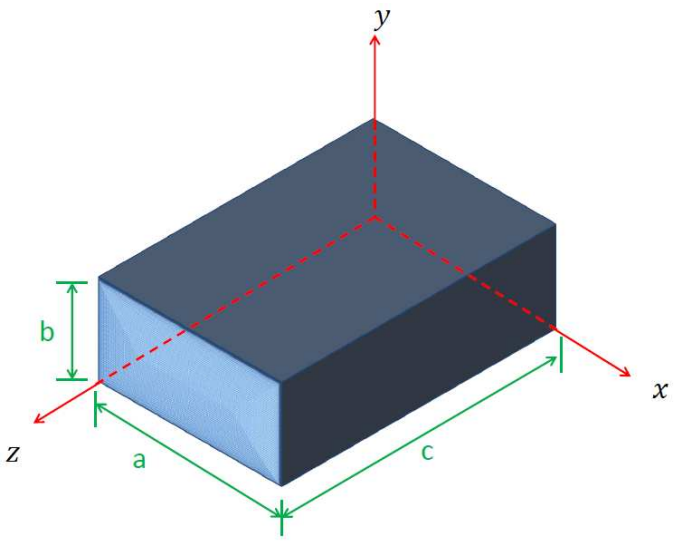

Figure 2.1: A rectangular cavity resonator

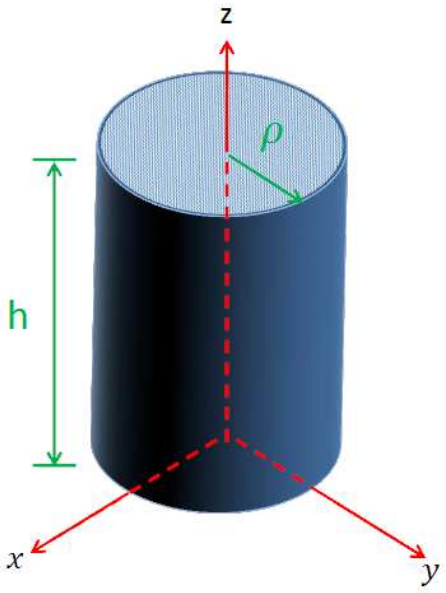

Figure 2.2: A circular cavity resonator

should be solved inside the cavity illustrated in Fig. 2.1 and the boundary conditions will be applied afterwards. The resonant frequency of the TE mode for the rectangular cavity is given by [5]:

$$
\begin{aligned}
(f_r)^{TE}_{mnp} &= \frac{1}{2\pi\sqrt{\mu\epsilon}}\sqrt{\left(\frac{m\pi}{a}\right)^2+\left(\frac{n\pi}{b}\right)^2+\left(\frac{p\pi}{c}\right)^2} \qquad (2.1)\\
& m = 0,1,2,\ldots\\
& n = 0,1,2,\ldots\\
& p = 1,2,3,\ldots
\end{aligned}
$$

where ϵ and μ are the relative permittivity and permeability of the material inside the cavity. The resonant frequency for the TM mode is given by [5]:

$$
\begin{aligned}
(f_r)^{TM}_{mnp} &= \frac{1}{2\pi\sqrt{\mu\epsilon}}\sqrt{\left(\frac{m\pi}{a}\right)^2+\left(\frac{n\pi}{b}\right)^2+\left(\frac{p\pi}{c}\right)^2} \qquad (2.2)\\
& m = 1,2,3,\ldots\\
& n = 1,2,3,\ldots\\
& p = 0,1,2,\ldots
\end{aligned}
$$

Assuming $c > a > b$; TE_{101} will be the dominant mode, whose resonant frequency is given by:

$$
(f_r)^{TE}_{101} = \frac{1}{2\sqrt{\mu\epsilon}}\sqrt{\left(\frac{1}{a}\right)^2+\left(\frac{1}{c}\right)^2} \qquad (2.3)
$$

2.2.2 Circular Cavity

Similar to the rectangular cavity, a circular cavity is constructed from a section of circular waveguide whose ends are closed. The resonant frequency of TE mode is [5]:

$$(f_r)^{TE}_{mnp} = \frac{1}{2\pi\sqrt{\mu\epsilon}}\sqrt{\left(\frac{\chi'_{mn}}{a}\right)^2 + \left(\frac{p\pi}{c}\right)^2} \tag{2.4}$$
$$m = 0, 1, 2, \ldots$$
$$n = 1, 2, 3, \ldots$$
$$p = 1, 2, 3, \ldots$$

where χ'_{mn} is the nth zero of the derivative of the Bessel function J_m of the first kind and of order m. The resonant frequency of the TM mode is [5]:

$$(f_r)^{TM}_{mnp} = \frac{1}{2\pi\sqrt{\mu\epsilon}}\sqrt{\left(\frac{\chi_{mn}}{a}\right)^2 + \left(\frac{p\pi}{c}\right)^2} \tag{2.5}$$
$$m = 0, 1, 2, \ldots$$
$$n = 1, 2, 3, \ldots$$
$$p = 0, 1, 2, \ldots$$

where χ_{mn} is the nth zero of the Bessel function J_m of the first kind and of order m.

2.3 Ferrite Materials

The magnetic properties of materials are primarily dependent to their electrons spin. The magnetic dipole moment of an electron due to its spin is:

$$m = \frac{qh}{4\pi m_e} = 9.27 \times 10^{-24} A - m^2 \tag{2.6}$$

where h is Plank's constant, q is the electron's charge and m_e is the mass of the electron.

There is an additional magnetic moment which is due to the effective current loop caused by the movement of the electron in an orbit around the nucleus. The

momentum generated in this manner is negligible in comparison with the momentum generated due to the spin of the electron.

In most of the solids, the overall magnetic momentum is negligible because the electron spins occur in pairs. In a magnetic material electrons' spins are unpaired; however, because of their random orientation, the overall momentum is still small. Therefore, applying an external magnetic field can align electron's momentum and finally result in a large moment.

The spin angular momentum s of an electron is given by [6],[7]:

$$s = \frac{h}{4\pi} \tag{2.7}$$

The ratio of the spin magnetic moment to the spin angular moment is referred to as *gyromagneticratio*:

$$\gamma = \frac{m}{s} = 1.759 \times 10^{11} \tag{2.8}$$

As indicated in Fig. 2.3, the following vector relation can be written:

$$\bar{m} = -\gamma \bar{s} \tag{2.9}$$

When a magnetic bias field of $\bar{H}_0 = \hat{z}H_0$ is applied to the ferrite material, the equation of the torque is:

$$\bar{T} = \bar{m} \times \bar{B}_0 = \mu_0 \bar{m} \times \bar{H}_0 \tag{2.10}$$

$$\bar{T} = -\mu_0 \gamma \bar{s} \times \bar{H}_0 \tag{2.11}$$

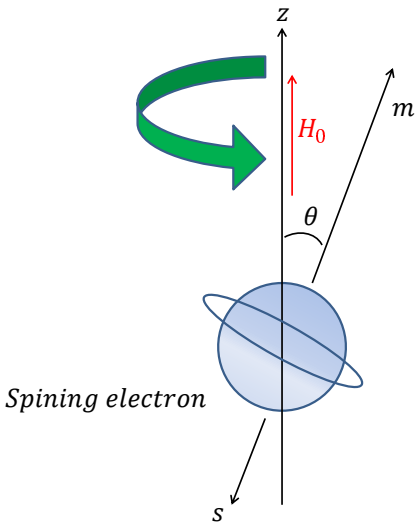

Figure 2.3: Spin magnetic dipole moment and angular momentum vectors for a spinning electron

Since the torque is related to the time rate of change of angular momentum, for a magnetic dipole moment of $\bar{m}$:

$$\frac{d\bar{s}}{dt} = \bar{T} = -\mu_0 \bar{m} \times \bar{H}_0 \tag{2.12}$$

and eventually

$$\frac{d\bar{m}}{dt} = -\mu_0 \gamma \bar{m} \times \bar{H}_0 \tag{2.13}$$

Rewriting this equation for different vector components, we have:

$$\frac{d\bar{m}_x}{dt} = -\mu_0 \gamma \bar{m}_y \bar{H}_0 \tag{2.14}$$

$$\frac{d\bar{m}_y}{dt} = -\mu_0 \gamma \bar{m}_x \bar{H}_0 \tag{2.15}$$

$$\frac{d\bar{m}_z}{dt} = 0 \tag{2.16}$$

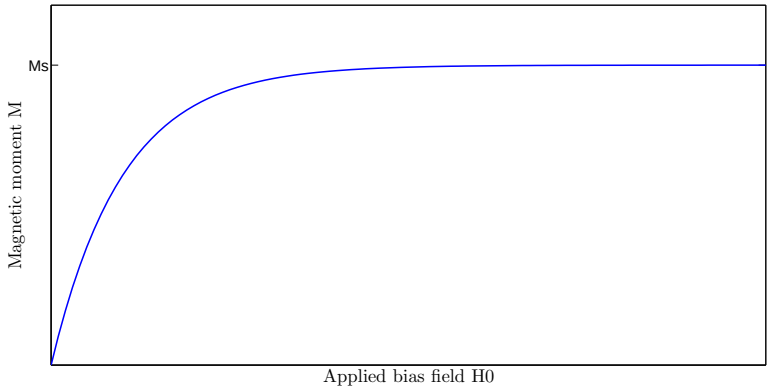

Figure 2.4: Magnetic moment of a ferrite material versus the biasing field

m_x and m_y can be obtained from (2.14) and (2.15):

$$m_x = A\cos(\omega_0 t) \tag{2.17}$$

$$m_y = A\cos(\omega_0 t) \tag{2.18}$$

where $\omega_0 = \mu_0 \gamma H_0$ is called precession frequency. If there are N unbalanced electron spins so that the total magnetization vector is:

$$\bar{M} = N\bar{m} \tag{2.19}$$

(2.13) reduces to:

$$\frac{d\bar{M}}{dt} = -\mu_0 \gamma \bar{M} \times \bar{H}_0 \tag{2.20}$$

As the strength of the biasing field (H_0) increases, more magnetic dipole moments align themselves with the the direction of the biasing field, until $\bar{M}$ reaches an upper limit. The material in such a state is said to be magnetically saturated and M_s is referred to as the *saturationmagnetization*. Fig. 2.4 illustrates how $\bar{M}$ reaches its upper limit.

Now, assume that the ferrite material is biased by the DC magnetic field of H_0 and an AC magnetic field is also applied. The total field is:

$$\bar{H}_t = H_0\hat{z} + \bar{H} \tag{2.21}$$

where $|\bar{H}| \ll H_0$. The total magnetization is:

$$\bar{M}_t = M_s\hat{z} + \bar{M} \tag{2.22}$$

where M_s is the DC saturation magnetization and $\bar{M}$ is the AC magnetization. Substituting (2.21) and (2.22) in (2.20) and solving for $\bar{M}$ results in:

$$\bar{M} = [\chi]\bar{H} = \begin{bmatrix} \chi_{xx} & \chi_{xy} & 0 \\ \chi_{yx} & \chi_{yy} & 0 \\ 0 & 0 & 0 \end{bmatrix} \bar{H} \tag{2.23}$$

where

$$\chi_{xx} = \chi_{yy} = \frac{\omega_0\omega_m}{\omega_0^2 - \omega_m^2} \tag{2.24}$$

$$\chi_{xy} = -\chi_{yx} = j\frac{\omega_0\omega_m}{\omega_0^2 - \omega_m^2} \tag{2.25}$$

and $\omega_0 = \mu_0\gamma H_0$, $\omega_m = \mu_0\gamma M_s$. The relationship between $\bar{B}$ and $\bar{H}$ is:

$$\bar{B} = \mu_0(\bar{M} + \bar{H}) = [\mu]\bar{H} \tag{2.26}$$

where the tensor permeability is given by:

$$[\mu] = \mu_0([U] + [\chi]) = \begin{bmatrix} \mu & j\kappa & 0 \\ -j\kappa & \mu & 0 \\ 0 & 0 & \mu_0 \end{bmatrix} \tag{2.27}$$

$$\mu = \mu_0(1 + \chi_{xx}) \tag{2.28}$$

$$\chi = -j\mu_0\chi_{xy} \tag{2.29}$$

If the DC magnetic field is in the x or y direction, the permeability tensor would be:

$$[\mu] = \begin{bmatrix} \mu_0 & 0 & 0 \\ 0 & \mu & j\kappa \\ 0 & -j\kappa & \mu \end{bmatrix} \tag{2.30}$$

$$[\mu] = \begin{bmatrix} \mu & 0 & -j\kappa \\ 0 & \mu_0 & 0 \\ -j\kappa & 0 & \mu \end{bmatrix} \tag{2.31}$$

The permeability tensors presented so far are valid when the applied magnetic field is in the z, x and y directions. The permeability tensor, when the ferrite is biased in an arbitrary direction, is expressed as [16], [17]:

$$[\mu_r] = \begin{bmatrix} \mu_{rxx} & \mu_{rxy} & \mu_{rxz} \\ \mu_{ryx} & \mu_{ryy} & \mu_{ryz} \\ \mu_{rzx} & \mu_{rxy} & \mu_{rzz} \end{bmatrix} \tag{2.32}$$

where

$$\mu_{rxx} = \mu_y + (1-\mu_z)\sin^2\theta\cos^2\phi + (\mu_z - \mu_y)\sin^2\theta \tag{2.33}$$

$$\mu_{rxy} = \frac{1-\mu_z}{2}\sin 2\theta \sin^2\phi + j\kappa\cos\theta \tag{2.34}$$

$$\mu_{rxz} = \frac{1-\mu_y}{2}\sin 2\theta\cos\phi - j\kappa\sin\theta\sin\phi \tag{2.35}$$

$$\mu_{ryx} = \frac{1-\mu_z}{2}\sin 2\theta\cos 2\phi - j\kappa\sin\theta\sin\phi \tag{2.36}$$

$$\mu_{ryy} = \mu_x + (1-\mu_z)\sin^2\theta\sin^2\phi + (\mu_z - \mu_x)\sin^2\theta \tag{2.37}$$

$$\mu_{ryz} = \frac{1-\mu_x}{2}\sin 2\theta\sin\phi + j\kappa\sin\theta\cos\phi \tag{2.38}$$

$$\mu_{rzx} = \frac{1-\mu_y}{2}\sin 2\theta\cos\phi + j\kappa\sin\theta\sin\phi \tag{2.39}$$

$$\mu_{rzy} = \frac{1-\mu_x}{2}\sin 2\theta\sin\phi - j\kappa\sin\theta\cos\phi \tag{2.40}$$

$$\mu_{rzz} = 1-(1-\mu_x\mu_y\sin^2\phi\cos^2\phi)\sin^2\theta \tag{2.41}$$

and

$$\mu_x = 1+\frac{\omega_x\omega_m}{\omega_r^2-\omega^2} \tag{2.42}$$

$$\mu_y = 1+\frac{\omega_y\omega_m}{\omega_r^2-\omega^2} \tag{2.43}$$

$$\mu_z = 1+\frac{\omega_z\omega_m}{\omega_r^2-\omega^2} \tag{2.44}$$

$$\kappa = \frac{\omega\omega_m}{\omega_r^2-\omega^2} \tag{2.45}$$

where

$$\omega_r^2 = \omega_z\sin^2\theta(\omega_x\sin^2\phi+\omega_y\cos^2\phi)+\omega_x\omega_y\cos^2\theta \tag{2.46}$$

$$\omega_x = \omega_0' + \omega_m N_x \tag{2.47}$$

$$\omega_y = \omega_0' + \omega_m N_y \tag{2.48}$$

$$\omega_z = \omega_0' + \omega_m N_z \tag{2.49}$$

$$\omega_0' = \gamma(H_i + j\frac{\Delta H}{2}) \tag{2.50}$$

$$\omega_m = \gamma 4\pi M_s \tag{2.51}$$

As it can be seen in (2.50), the frequency is a complex variable. A complex frequency expresses the loss of ferrite material which is related to its linewidth (ΔH). The linewidth is defined as the width of the curve of the imaginary part of χ_{xx} versus H_0, when it has decreased to half its peak value [8]. This loss factor reduces the gain of the CBS antenna and can be alleviated by biasing the ferrite material. Also note that this loss does not take into account the dielectric loss of ferrite material.

Chapter 3

Modeling of the Cavities, Electromagnet, Permanent Magnets and Biasing Magnetic Field

3.1 Introduction

Two common cavity-backed slot antenna geometries are considered in this thesis: rectangular and circular cross-sectional. The ferrite material that was used is G-475 ($4\pi M_s = 475$, $\Delta H = 45$ @ 9.4 GHz, $g = 2.01$, $\epsilon_r = 13.35$), whose characteristics can be found in [9]. To consider the non-uniformity of the magnetic field distribution inside the cavity, Ansys Maxwell 3D [10] is used to simulate the DC biasing of ferrite material. The analysis of the radiation characteristics of the ferrite loaded CBS antenna is performed using commercial software Ansys HFSS v.13.0. Simulations in HFSS are based on the Finite Element Method. The results of Maxwell 3D are imported into HFSS to investigate the impact of the magnetic field non-uniformity on the RF characteristics.

3.2 Rectangular Cross-Section Cavity

The rectangular CBS antenna considered in this thesis is based on an aluminum cavity with dimensions of 7.62 cm $\times$ 1.27 cm $\times$ 5.08 cm. The 3D CAD geometry of the rectangular cross-section CBS antenna and coordinate system are illustrated in Fig. 3.1. The top and side views of the actual rectangular cross-section CBS antena employed in the simulations and measurements are shown in Fig. 3.2. In [1], the antenna was loaded with one layer of ferrite material (the red slab in Fig. 3.1) placed on top of a triangular probe, which was soldered to the inner conductor of 50 Ω coaxial cable; however, the sample of ferrite material will not be at the same location in this thesis.

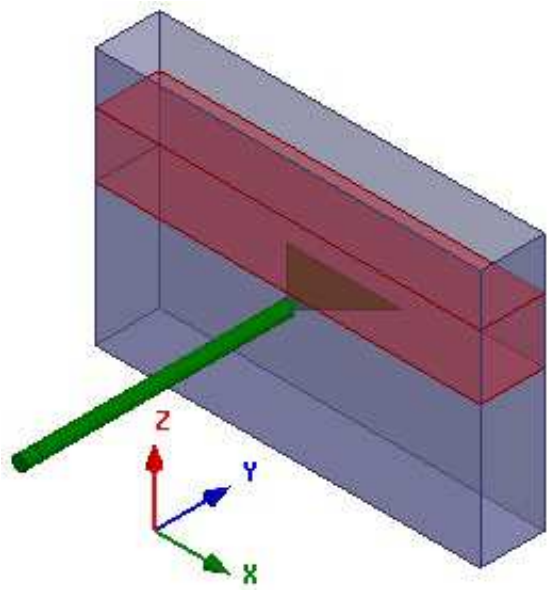

Figure 3.1: General 3D CAD geometry of the rectangular cross-section CBS antenna with ferrite material (red slab) on top of the probe

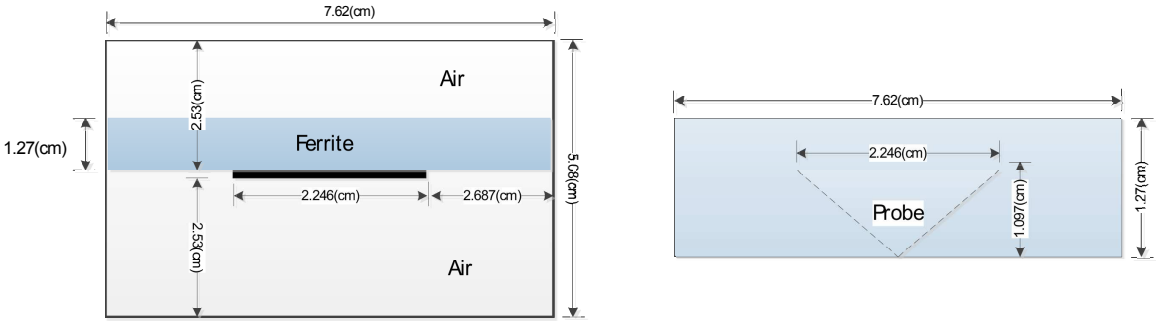

Figure 3.2: Left figure; side view of rectangular cross-section cavity, right figure; top view of rectangular cross-section cavity

3.3 Circular Cross-Section Cavity

The next geometry of the CBS antenna is based on an aluminum cube of side 5.08 cm, inside which a circular cylindrical cavity of diameter 3.81 cm is carved. A wire type of probe is used to excite the antenna, which is again soldered to the center conductor of 50 Ω coaxial cable. The 3D CAD geometry of the circular cross-section CBS antenna and the coordinate system are illustrated in Fig. 3.3. The top and

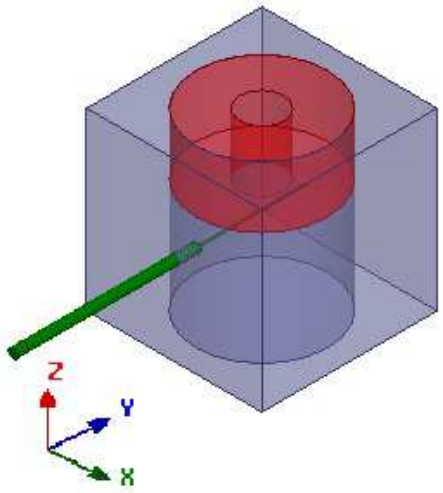

Figure 3.3: General 3D CAD geometry of the circular cross-section CBS antenna with ferrite material (red slab) on top of the probe

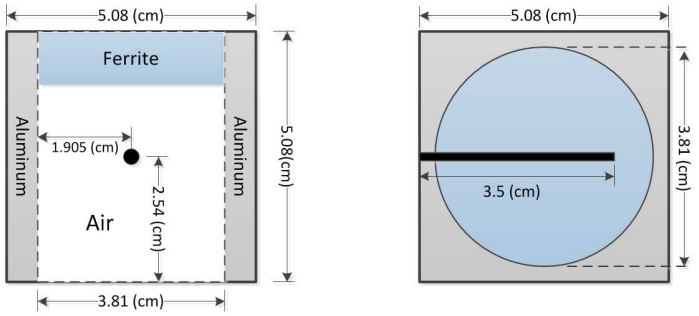

Figure 3.4: Left figure; side view of circular cross-section cavity of height 2 inches, right figure; top view of circular cross-section cavity of height 2 inches

side views of the actual circular cross-section CBS antenna employed in this thesis are shown in Fig. 3.4. The other geometry of the circular cross-section CBS antenna which is investigated in this thesis is illustrated in Fig. 3.5. As it can be seen, its geometry is very similar to that of Fig. 3.4. The only difference is its height which is 1 inch.

3.4 Electromagnet and Permanent Magnet

The ferrite material inside either of the cavities is usually biased by the external magnetic field produced by an electromagnet; however, two sets of permanent magnets

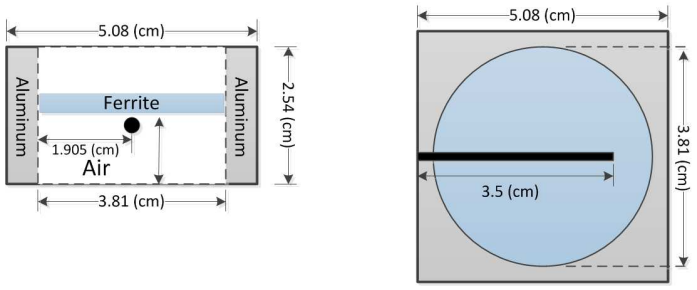

Figure 3.5: Left figure; side view of circular cross-section cavity of height 1 inch, right figure; top view of circular cross-section cavity of height 1 inch

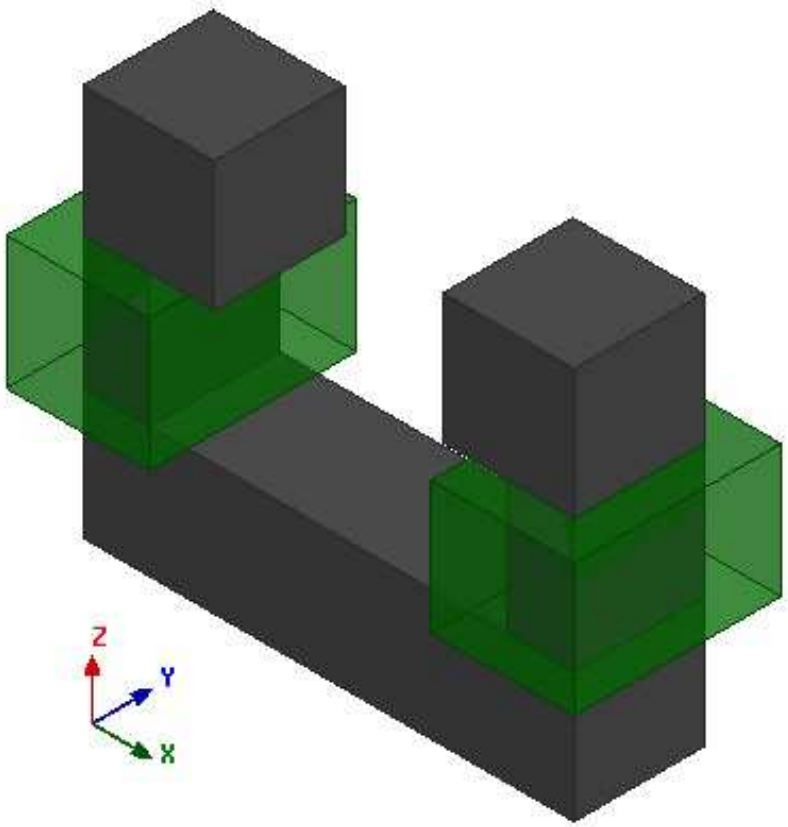

Figure 3.6: 3D CAD geometry of the electromagnet

were used for measurements presented in this thesis. The 3D CAD geometry of the electromagnet is illustrated in Fig. 3.6. The physical geometry of the electromagnet is shown in Fig. 3.7. The entire structure consists of the iron (black) and two coils (green). In Ansys Maxwell 3D, the arms are modeled as steel-1008 and the cores

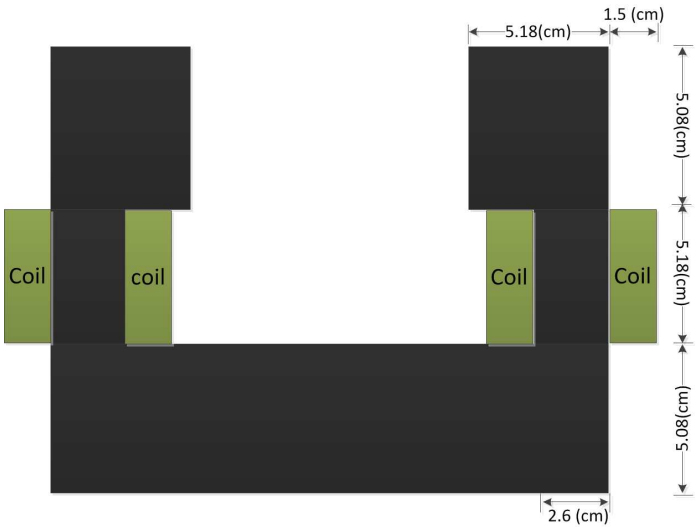

(a)

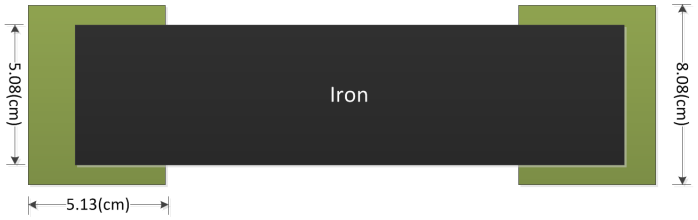

(b)

Figure 3.7: Geometry of the electromagnet: (a) side view (b) top view

are modeled as copper whose B-H curve is taken from Ansys Maxwell 3D material library. The dimensions of the permanent magnets are 2.4 cm $\times$ 5.08 cm $\times$ 5.08 cm, and they have been modeled as NdFe35.

Chapter 4

Simulations and Measurements

4.1 Introduction

The main goal of this chapter is the demonstration of the impact of the shape and the position of the ferrite material on the performance of the cavity-backed slot antenna. The first step is to find out the reasons for the low gain and poor impedance match of the ferrite-loaded CBS antenna which was reported in [1]. To overcome these drawbacks, other configurations of ferrite material will be suggested.

Since the performance of the antenna is a function of the current in the electromagnet's coil, the number of its turns must be specified. To prevent from restricting our design to the certain number of turns around the electromagnet's arms, the magnitude of the magnetic field at the center point of the cavity will instead be specified, which is represented as H_a. It should be noted that all of the gains in this paper do not take into account the impedance mismatch.

4.2 Rectangular Cross-Section Cavity

4.2.1 Ferrite shaping and positioning

The position and the shape of ferrite material have impacts on the figures-of-merit of the CBS antenna. Simulations show that the empty CBS antenna resonates at 2.13 GHz with a gain of 4 dBi and an S_{11} of -8 dB. The ferrite sample will be located in the CBS antenna in the following sections.

Ferrite Sample on Top of the Probe

The main drawbacks of the ferrite configuration reported in the Fig. 2 of [1] are the low gain and poor impedance match. For an H_a of about 600 Oe, the gain is -2 dBi at 0.95 GHz. To determine how to overcome this problem, it is necessary to analyze the electric field distribution inside the cavity. The cavity in this thesis can be viewed

as an approximate model of a stripline, as it has been modeled in Fig. 8-53 of [5]. The major difference is the opening on the top wall of the CBS antenna which causes stronger fields at the aperture. The equivalent capacitances of the CBS antenna can still be modeled as in Fig. 8-53 of [5]. To assess the performance of the cavity, the internal field distribution should be investigated. The electric field distribution of Fig. 2 of [1] on the YZ (end view of cavity) and XZ (side view of cavity) planes is computed and illustrated in Fig. 4.1.

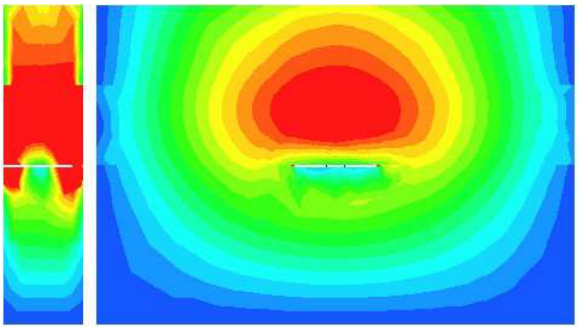

Figure 4.1: Electric field distribution of Fig. 2 of [1] on the YZ (left figure; end view of cavity) and XZ (right figure; side view of cavity) planes

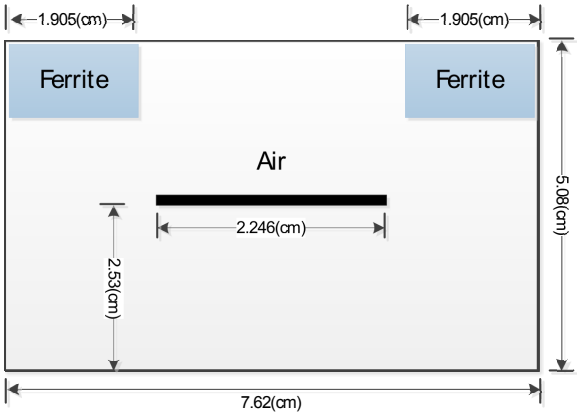

Figure 4.2: Removal of the center part of the ferrite sample (XZ-plane; side view)

It is apparent that the electric field intensity at the aperture of the cavity is lower than that in the area near the probe. The other point of interest is the electric field intensity at the corners of the cavity. Since the permittivity of air is

much smaller than that of the ferrite, the electric fields are attracted toward the ferrite sample. Now, placing the ferrite material on top of the probe causes the stronger fields to concentrate near the center of the cavity. Having weaker fields at the corners decreases the equivalent fringing capacitances designated in Fig. 8-53 of [5], and they even become smaller than those of the empty cavity. Such an electric field distribution, with weak electric fields both at the aperture and corners, leads to a low gain and impedance mismatch.

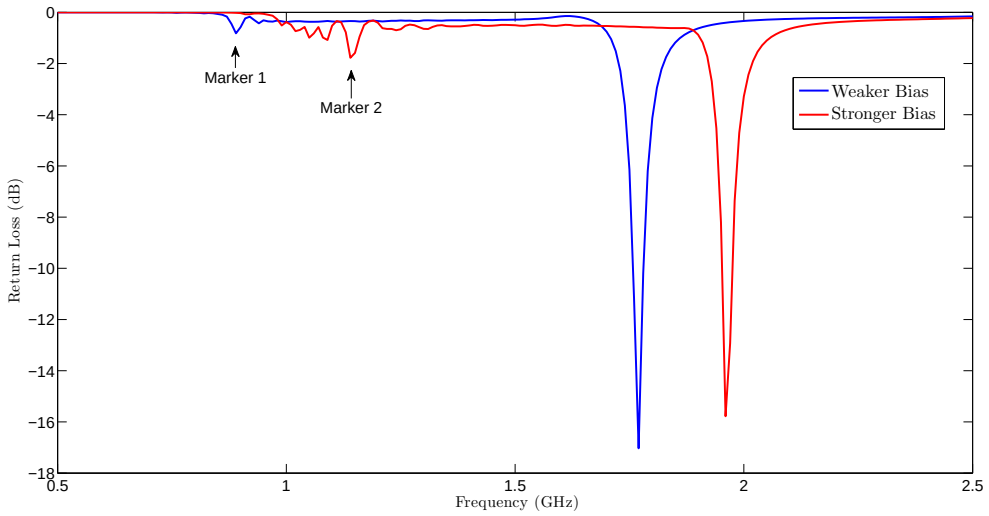

Figure 4.3: The new dominant mode becomes more apparent as H_a increases.

Ferrite Samples at the Aperture of the Cavity

The first attempt to increase the gain of the antenna was to examine the influence of an open aperture and the relative placement of the ferrite material, as shown in Fig. 4.2, where the ferrite material is placed at the opening and its center part is removed. Simulations of the geometry of Fig. 4.2, for different magnetic bias fields, indicated that for weaker fields the dominant resonant frequency is about 2 GHz (marker1). This resonant frequency is much higher than that of the geometry investigated in [1]. To maintain the resonant frequency low, larger currents were applied to the coil

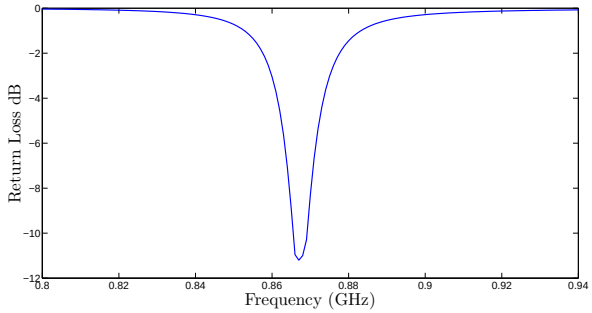

(a)

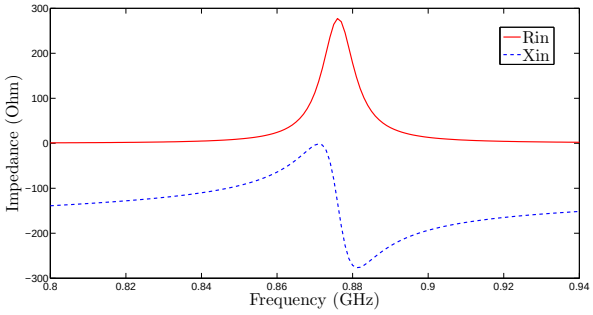

(b)

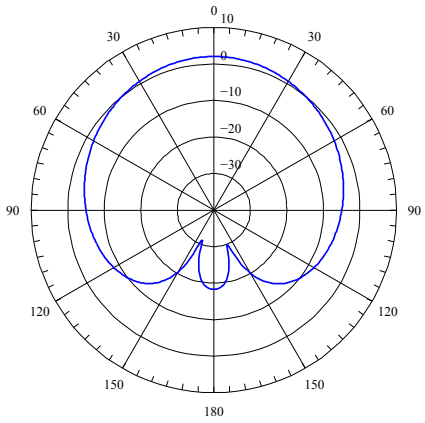

(c)

Figure 4.4: Radiation characteristic of Fig. 4.2: (a) Return loss (b) Input impedance (c) Gain pattern on the E-plane (YZ plane) at 1.0 GHz

of the electromagnets, and finally a new mode appeared at a lower frequency range (marker2). Fig. 4.3 demonstrates how the new resonant frequency becomes more apparent as the coil current increases. This means that for the stronger biasing the new mode should be considered as the dominant resonant frequency. Introducing an open aperture, which can be interpreted as removing part of the lossy material in the direction of radiation, resulted in a gain of about 2 dBi at 1.26 GHz. Increasing the magnitude of the applied magnetic field, and having the ferrite more uniformly biased, produces an S_{11} of about -12 dB. However, due to the reduction of the size of the ferrite material in the geometry of Fig. 4.2, the sensitivity of the resonant frequency to the applied magnetic field was reduced. The return loss and input impedance as a function of frequency and gain pattern of Fig. 4.2 on the E-plane (YZ plane) at 1 GHz are illustrated in Fig. 4.4.

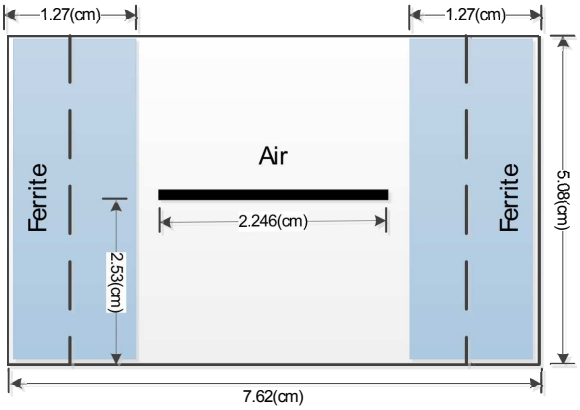

Figure 4.5: The rectangular cross-section cavity with ferrite material on its sides (XZ-plane; side view)

Ferrite Samples on the Sides of Cavity

One of the solutions to overcome the reduction in the resonant frequency sensitivity is to introduce more ferrite material on both sides of the cavity, as shown in Fig. 4.5. In this manner, the aperture is still open and a larger portion of the cavity is occupied with ferrite material.

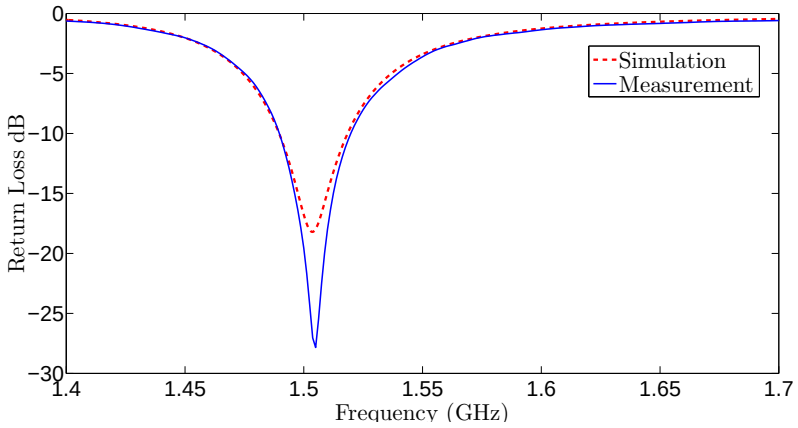

(a)

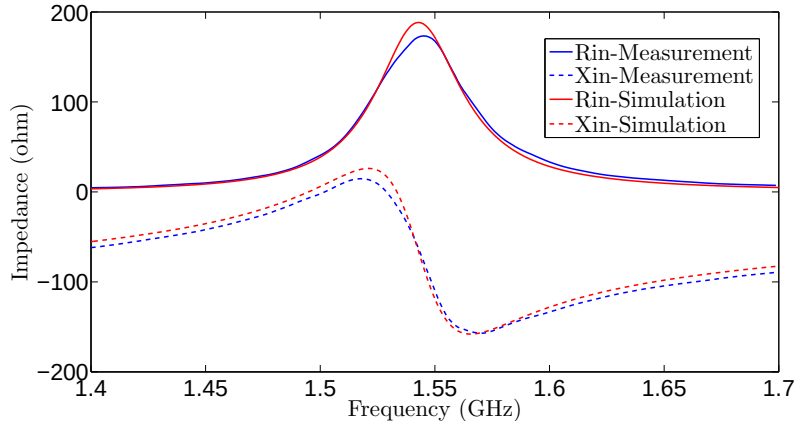

(b)

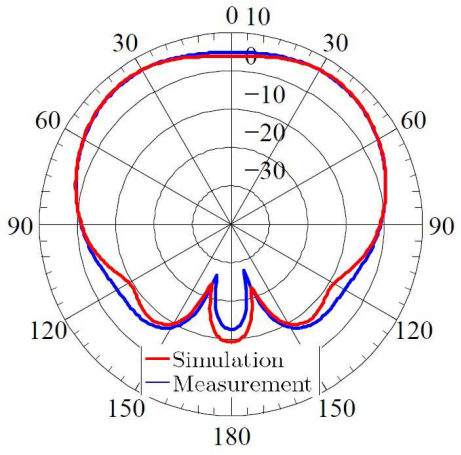

(c)

Figure 4.6: Simulations and measurements: (a) Return loss (b) Input impedance (c) E-plane (YZ plane) pattern at 1.51 GHz

Simulations for the geometry of Fig. 4.5 indicated that an S_{11} lower than -15 dB is achievable. The smallest H_a needed to have such a match is about 590 Oe. For this excitation, the antenna resonates at 1.27 GHz with a gain of about 4.4 dBi and an S_{11} of about -15.28 dB. Increasing the current even further (i.e. increasing H_a) results in a better impedance match. Setting the current to a value such that H_a is equal to 855 Oe, the resonant frequency shifts upwardly to 1.36 GHz. The gain and the return loss at the mentioned frequency are 5.2 dB and -20 dBi, respectively.

This geometry was also subjected to measurements. To measure complete amplitude patterns in the EMAC facility required that the antenna under test be turned on for a long time (typically 3 hours). Because the coil in the electromagnet was overheating when the current was high and applied for hours, the permanent magnets were used, instead of the electromagnet, to bias the ferrite material and perform the measurements. In Ansys Maxwell 3D, the permanent magnet was modeled as NdFe35. Fig. 4.6 displays predicted and measured input impedance, S_{11} and gain for the geometry of Fig. 4.5. It is apparent that a very good agreement between simulations and measurements has been achieved. It should be noted that the electrical/magnetic parameters of the ferrite material were tweaked due to the tolerances given in the company catalog [9], in order to achieve a better agreement between the measurements and simulations.

All of the figures-of-merit have improved for the geometry of Fig. 4.5. However, the amount of ferrite material used in the design of Fig. 4.5, as compared to Fig. 4.2, increased substantially. Therefore, it would be of interest to investigate the impact of different parts of ferrite material on the antenna performance and remove any parts that may not be necessary. Hence, it is prudent to examine the permeability of the ferrite for the geometry of Fig. 4.5. Fig. 4.7 shows the static relative permeability of the ferrite material subjected to a DC applied magnetic field, H_a, of

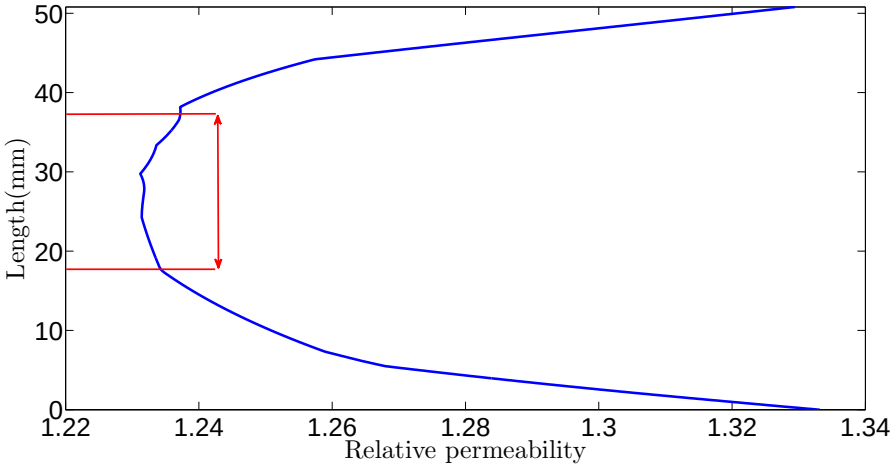

Figure 4.7: The permeability of ferrite material along the dashed lines of Fig. 4.5

590 Oe. The permeability inside the ferrite is plotted along the vertical dashed line shown in Fig. 4.5. As can be seen in Fig. 4.7, the permeability in the vicinity of the probe is closer to unity, as indicated by the red arrow; this area is more uniformly biased as well. This implies that the ferrite material in this area behaves more like a dielectric, rather than a ferrite, so its effectiveness on the tunability of the antenna diminishes. It would then be interesting to remove this part of the ferrite and observe its impact on the radiation characteristics of the CBS antenna. This is discussed in the section that follows.

Ferrite Samples at the Corners of the Cavity

After removing the part of the ferrite material in the region indicated by the red arrow in Fig. 4.7, the cavity is loaded with ferrite material only at its corners. This geometry is illustrated in Fig. 4.8. For an H_a of 590 Oe, the antenna resonates at 1.46 GHz. At this frequency, the S_{11} and gain are -18.23 dB and 4 dBi, respectively. So a -15 dB S_{11} occurs for weaker magnetic fields and at a lower frequency relative to the geometry of Fig. 4.5. Increasing H_a to 855 Oe, the antenna resonates at 1.57 GHz, the S_{11} is equal to -27.8 dB, and the gain is approximately 3.8 dBi. The S_{11}, as

a function of the frequency and the gain pattern on E-plane (YZ plane) at 1.45 GHz and 1.57 GHz are illustrated in Fig. 4.9.

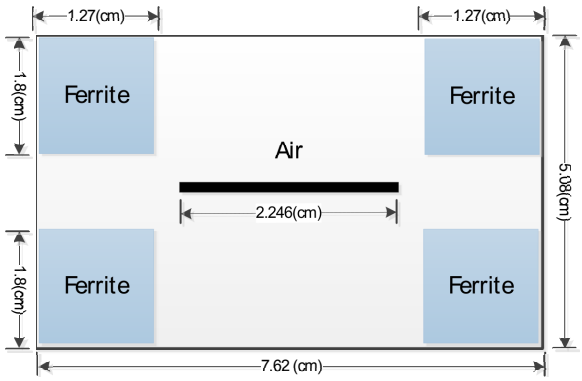

Figure 4.8: The rectangular cross-section cavity with ferrite samples at its corners (XZ-plane; side view)

Placing the ferrite material in different locations inside the cavity changes its electric field distribution which impacts its input impedance and gain. The capacitances can still be modeled as they have been in Fig. 8-53 of [5].

The field distribution of the cavity with ferrite configurations illustrated in Fig. 4.8 on YZ and XZ planes is shown in Fig. 4.10. In the configuration of Fig. 4.8, the ferrite samples attract the electric fields to the corners of the cavity which increases the fringing capacitances and eventually decrease the input reactance of the antenna. Hence a better impedance match is observed. Since stronger fields occur at the aperture, a larger radiation resistance also results. When the cavity is loaded with ferrite material on its sides as illustrated in Fig. 4.5, although the gain is higher than the geometry reported in Fig. 2 of [1], the fringing capacitances are again smaller when compared with the configuration in which the samples are at the corners. Hence an S_{11} lower than -15 dB can be achieved by the geometry illustrated in Fig. 4.8 for weaker magnetic excitations.

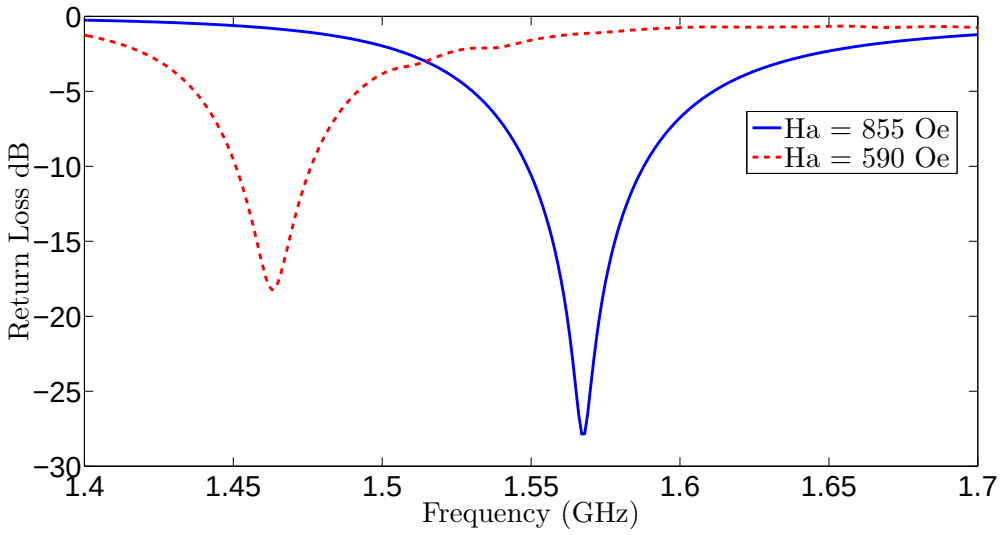

(a)

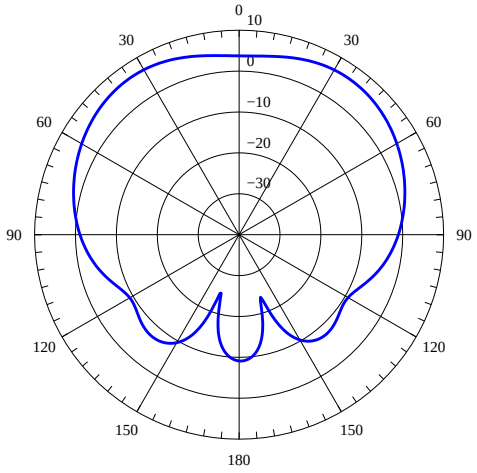

(b)

Figure 4.9: Simulations: (a) The change in the resonant frequency for different excitations (b) E-plane pattern of the geometry of Fig. 4.8

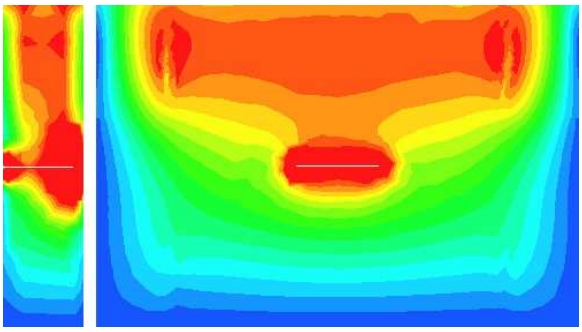

Figure 4.10: Electric field distribution of Fig. 4.8 on the YZ (left figure; end view of cavity) and XZ (right figure; side view of cavity) planes

4.2.2 The length and angle of the triangular probe

Appropriate locations and shapes for the ferrite material inside the cavity have been determined so far. Now, since the current distribution depends on the geometry of the probe, it would be of interest to investigate the impact of the probe's geometry on the performance of the antenna. Hence systematic, sets of simulations are performed. The effect of the length and the angle of the triangular probe shown in Fig. 3.2 are examined in the sections that follow. The ferrite configuration is the same as Fig. 4.8.

Probe angle

To observe the impact of probe angle on the radiation characteristics, the length (h) of the probe is maintained constant and θ is varied. Fig. 4.11 illustrates how the angle of the probe is changing. Fig. 4.12 shows the impact of the probe's angle on return loss. As it can be seen, the resonant frequency increases as the probe's angle decreases. Generally, a more acceptable impedance match is obtained when the angle is between 60 to 80 degrees. For the geometry of Fig. 4.8, the best impedance match occurred when θ was about 65 degrees. Simulations show that the gain of the antenna is not really changing with variation of the probe angle; therefore they are

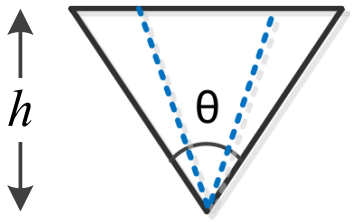

Figure 4.11: Angle θ is varied to observe the impact of angle on the radiation characteristics

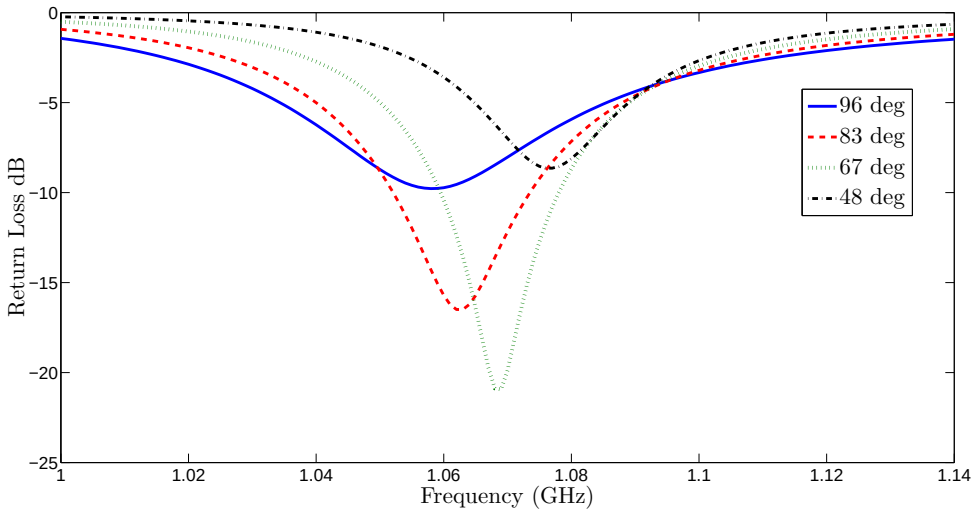

Figure 4.12: Return loss of the cavity configuration of Fig. 4.8 for different probe angles

not presented here again.

Probe length

The other parameter in the probe design, which may affect the figures-of-merit of the antenna, is its length (h). To observe the impact of different lengths, θ is set to the optimum value presented in the previous section and h will be varied from 0.91 cm to 1.12 cm. Fig. 4.13 demonstrates how the geometry of the probe is varied.

Simulations show that the optimum length of the probe is 1.06 cm, for which a return loss of about -50 dB can be obtained. Simulation results for some of these lengths are displayed in Fig. 4.14.

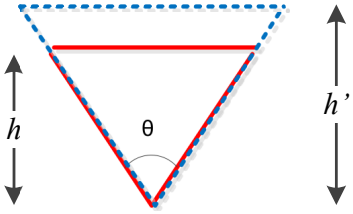

Figure 4.13: $\theta = 65°$, h is changing to observe the impact of the probe length on the radiation characteristics of the CBS antenna

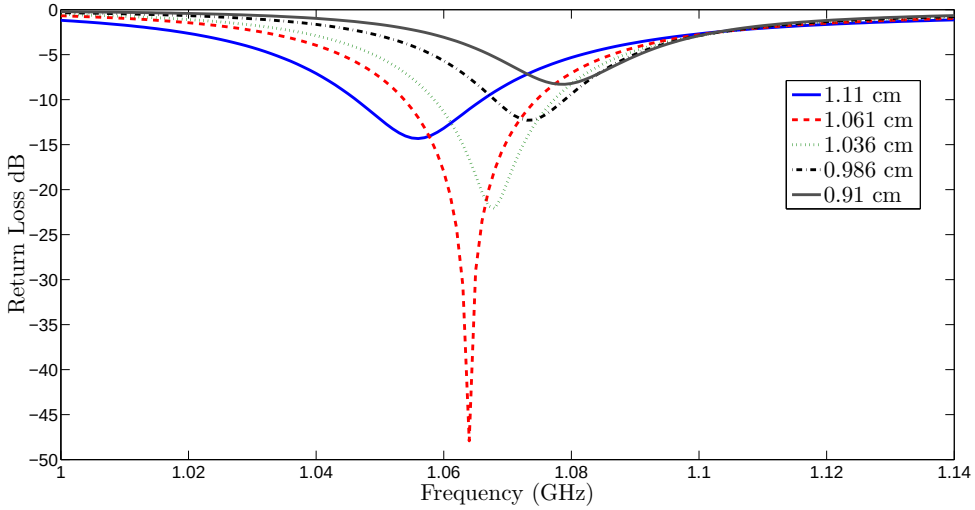

Figure 4.14: Return loss of the cavity configuration shown in Fig. 4.8 for different probe lengths

4.2.3 Tunable Bandwidth

In this thesis, the lower and higher frequencies of the -15 dB tunable bandwidth are defined as:

- f_L: The resonant frequency at which the S_{11} is equal or less than -15 dB, meanwhile H_a must be as small as possible.
- f_H: The resonant frequency of the antenna, when H_a is 855 Oe.
- The tunable bandwidth will be defined as: $BW = f_L - f_H$.

Based on this definition, the tunable bandwidth for the geometry of Fig. 4.5 is about 90 MHz, while that of the geometry in Fig. 4.8 is about 120 MHz. The probe geometry is the same as Fig. 3.2.

It must be mentioned that increasing the current results in higher resonant frequencies. However, a maximum value was considered so that we can compare the sensitivity of different ferrite configurations within a certain range of current and also the impedance match of the antenna for different geometries with the same excitations; H_a of 855 Oe corresponds to 4.5 A.

4.3 Circular Cross-Section Cavity; Two-inch height

4.3.1 Ferrite shaping and positioning

Similar to the rectangular cross-section cavity, the position and the shape of the ferrite material inside the circular cross-section cavity have an impact on the figures-of-merit of the CBS antenna. Simulations show that the antenna of Fig. 3.4 (without the ferrite material) resonates at 6 GHz with a gain of about 7 dBi and an S_{11} of about -24 dB. Fig. 4.15 illustrates its return loss and gain pattern on the E-plane (YZ plane) at 6 GHz. Now that the radiation characteristic of the empty circular-cross section cavity has been determined, let us place a ferrite specimen on top of the probe and investigate the antenna's performance.

Ferrite Material on Top of the Probe

The geometry in which the ferrite is placed on top of the probe is illustrated in Fig. 4.16. The S_{11} and gain pattern of the geometry of Fig. 4.16 is shown in Fig. 4.17. As it can be seen, new modes have appeared at lower frequencies which are associated with the ferrite material. The dominant resonant frequency has decreased to 3 GHz. The gain and return loss at this frequency are -9.4 dBi and -5 dB, respectively. So it can be concluded that, similar to the previously reported rectangular cross-section

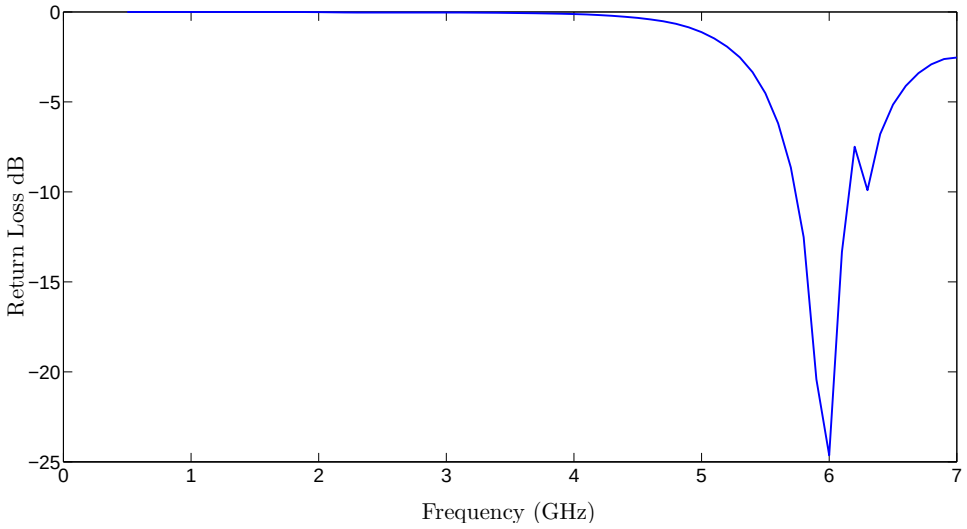

(a)

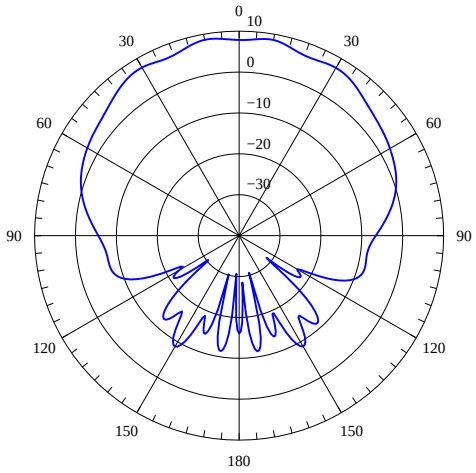

(b)

Figure 4.15: (a) Return loss of Fig. 3.4 (b)E-plane (YZ plane) pattern of the geometry of Fig. 3.4

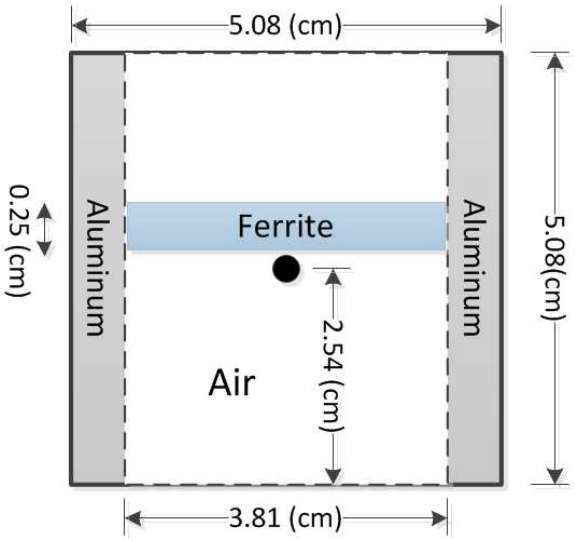

Figure 4.16: Side view (XZ plane) of the circular cross-section cavity with ferrite material on top of the probe

CBS antennas, placing the ferrite material on top of the probe in the circular cross-section cavity leads to a low gain and poor impedance match. The design procedure which was presented for the rectangular based CBS antenna in previous sections will be followed for the circular based CBS antenna to observe if the same trends exist. The electric field distribution of Fig. 4.16 on the YZ (end view of the cavity) and XZ (side view of the cavity) planes is computed and illustrated in Fig. 4.18. Similar to the rectangular cross-section, the electric field intensity at the aperture and the corners of the CBS antenna is lower than that in the area close to the probe. Such an electric field distribution leads to a poor radiation and impedance match.

Ferrite Material at the Aperture

To examine the impact of an open aperture, the ferrite material is placed at the opening and the center part of it is removed. This ferrite configuration is shown in Fig. 4.19. Simulations indicate that the gain of the antenna increases substantially relative to that of Fig. 4.16. However, the impedance match is still not acceptable. The S_{11} and the gain pattern of the Fig. 4.19 on the E-plane (YZ plane) at 3 GHz

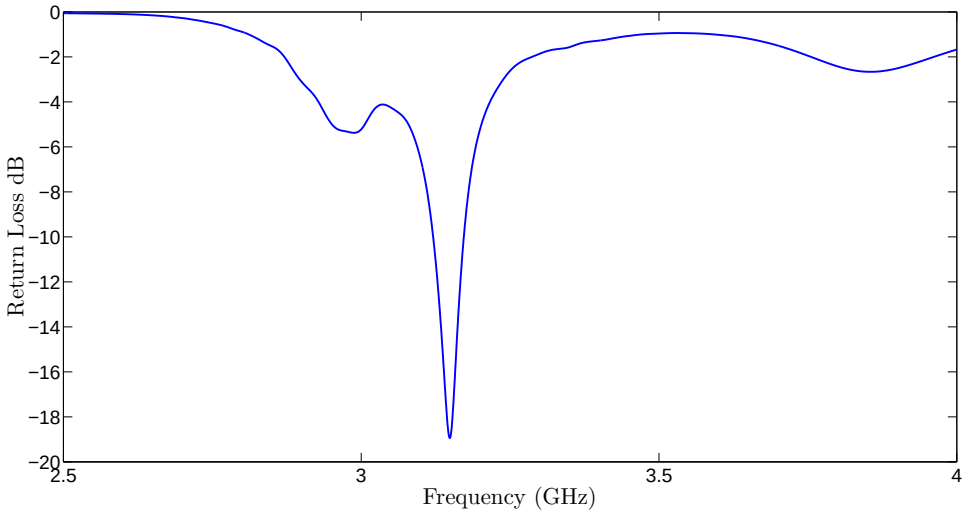

(a)

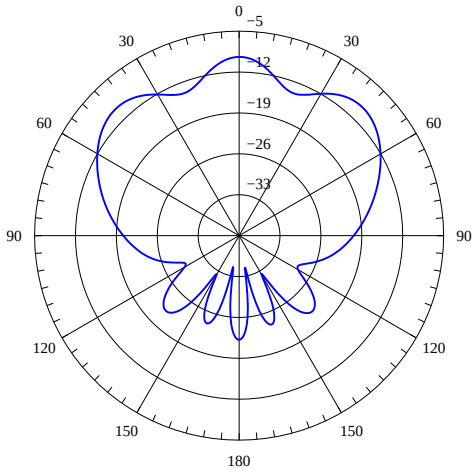

(b)

Figure 4.17: (a) Return loss of Fig. 4.16 (b) E-plane (YZ plane) pattern of the geometry of Fig. 4.16

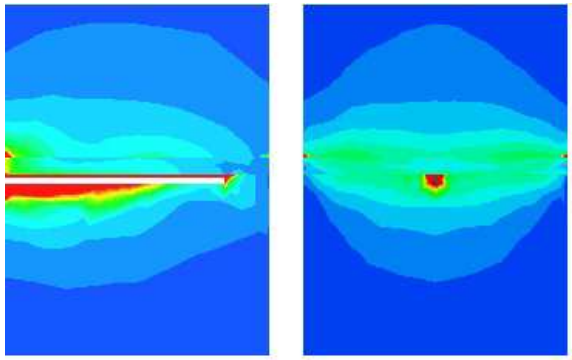

Figure 4.18: Electric field distribution of Fig. 4.16 on the YZ (left figure; end view of cavity) and XZ (right figure; side view of cavity) planes

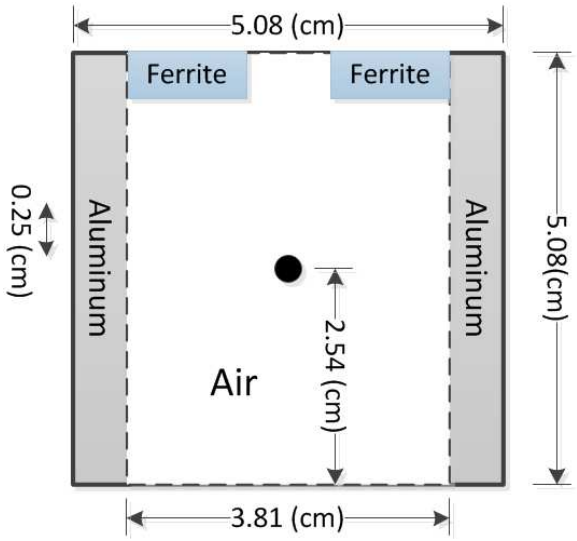

Figure 4.19: Removal of the center part of ferrite sample (XZ-plane; side view)

are illustrated in Fig. 4.20. The other problem of the geometry of Fig. 4.2 exists here as well; the small amount of ferrite material has lessened the sensitivity of the resonant frequency to the magnetic field bias.

Ferrite Material at the Aperture and on the Bottom

To overcome the reduction in the resonant frequency sensitivity, more ferrite material in the cavity is required. The placement of the ferrite material in the cavity should be such that it does not decrease the gain and also to improve the impedance match.

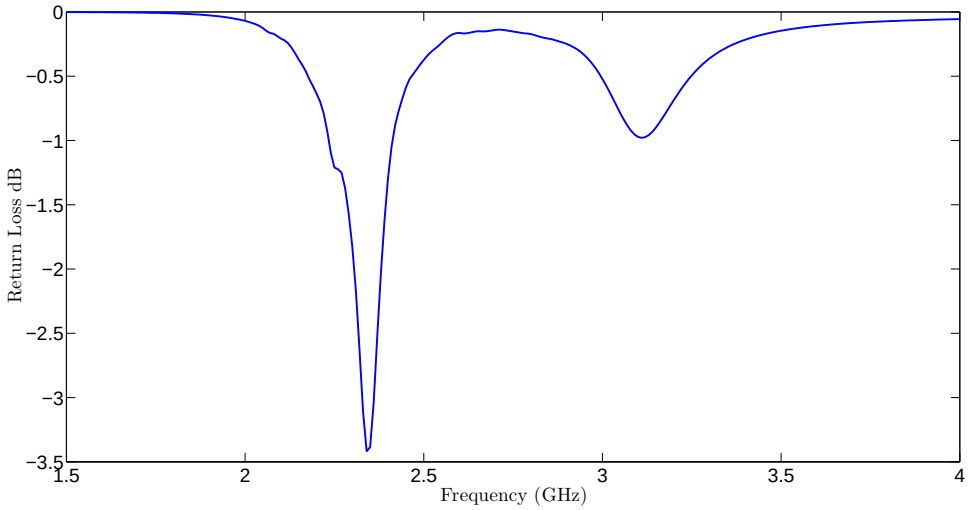

(a)

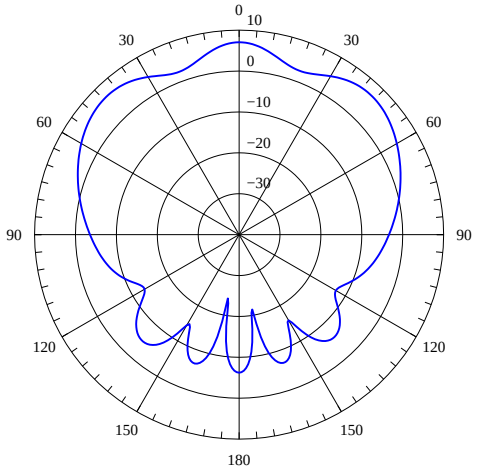

(b)

Figure 4.20: (a) Return loss of Fig. 4.19 (b)E-plane (YZ plane) pattern of the geometry of Fig. 4.19

To maintain the gain high and achieve an acceptable impedance match, the aperture should remain open, meanwhile the electric fields at the corners of the cavity should become more intense. Such geometry is illustrated in Fig. 4.21.

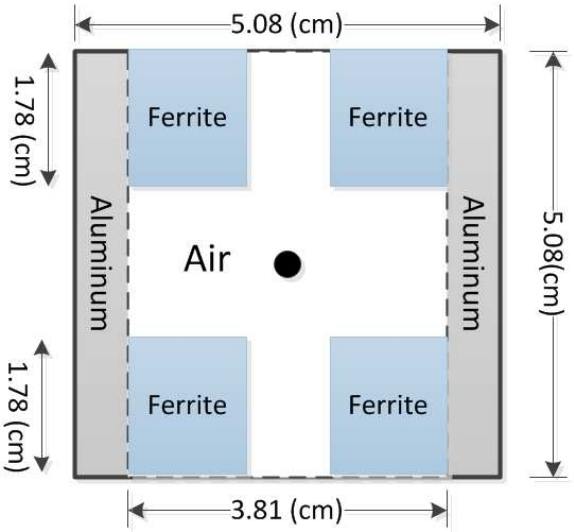

Figure 4.21: Circular cross-section cavity with ferrite material at the aperture and on the bottom

Simulations for the geometry of Fig.4.21 indicate that an S_{11} lower than -15 dB is achievable for this ferrite configuration. The smallest H_a needed to have such a match is about 610 Oe. For this excitation, the antenna resonates at 1.4 GHz with a gain of about 2 dBi and an S_{11} of about -16 dB. Increasing the current to a value such that H_a is equal to 855 Oe, the resonant frequency shifts upwardly to 1.54 GHz. The gain and return loss at the mentioned frequency are 4.17 dBi and -15 dB, respectively. The simulation results of the earlier case (H_a = 600 Oe) are presented in Fig. 4.22.

The electric field distribution of the cavity with the ferrite configuration illustrated in Fig. 4.21 on YZ and XZ planes is shown in Fig. 4.23. As it was expected, the stronger electric fields are occurring at the aperture and the corners of the cavity. Hence a higher gain (because of the strong electric field at the aperture) and better impedance match (because of the strong electric field at the corners) is achieved.

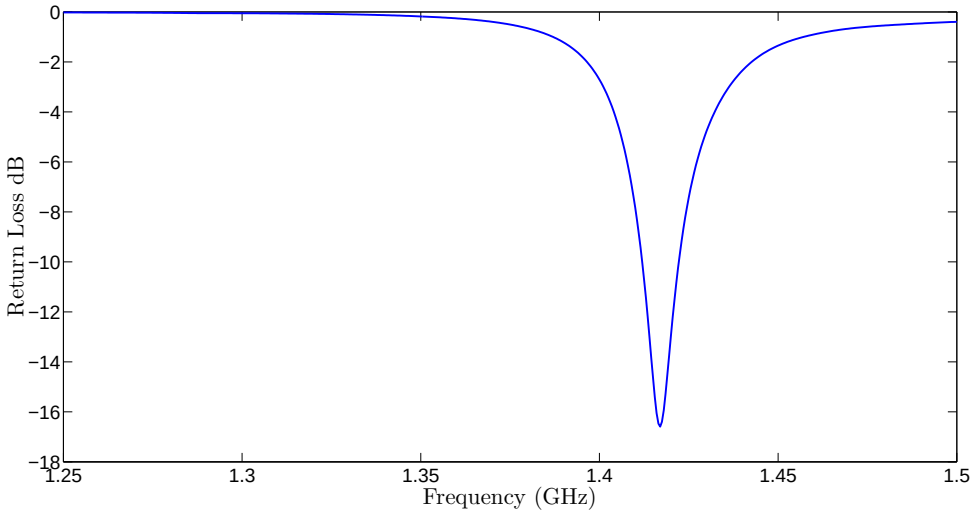

(a)

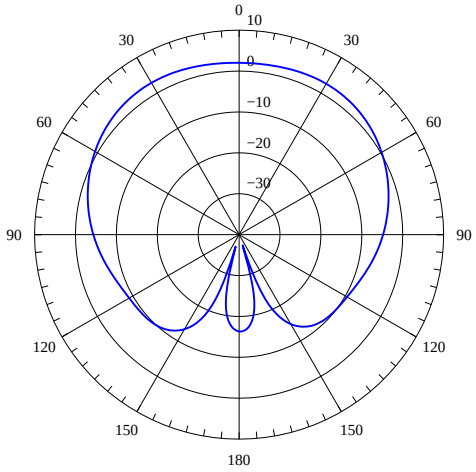

(b)

Figure 4.22: (a) Return loss of Fig. 4.21 (b) E-plane (YZ plane) pattern of the geometry of Fig. 4.21

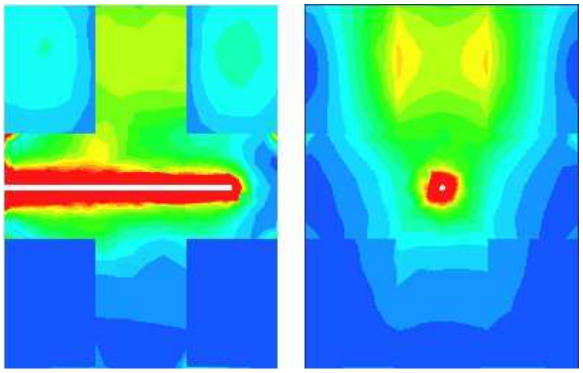

Figure 4.23: Electric field distribution of the cavity configuration shown in Fig. 4.21 on the YZ (left figure; end view of cavity) and XZ (right figure; side view of cavity) planes

This geometry was also subjected to measurements; however, due to the limitation in the availability of ferrite, the geometry is slightly different form that of Fig. 4.21. This geometry is illustrated in Fig. 4.24.

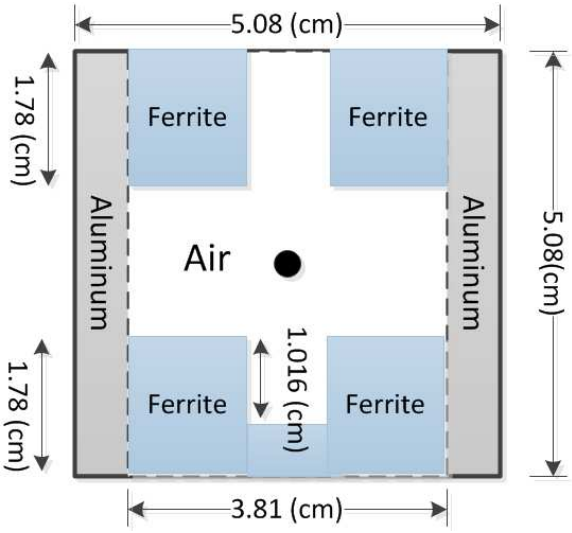

Figure 4.24: The ferrite configuration, on which the measurement for the circular cross-section cavity (of height 2 inches) was performed

Fig. 4.25 illustrates the results obtained from the measurements and simulations. Comparing these two sets of results indicates a good agreement between measurements and simulations.

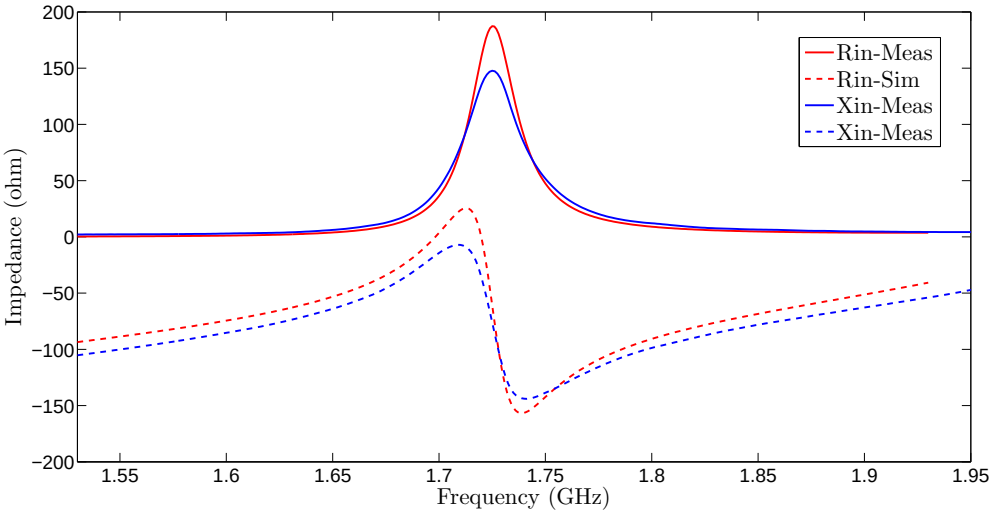

(a)

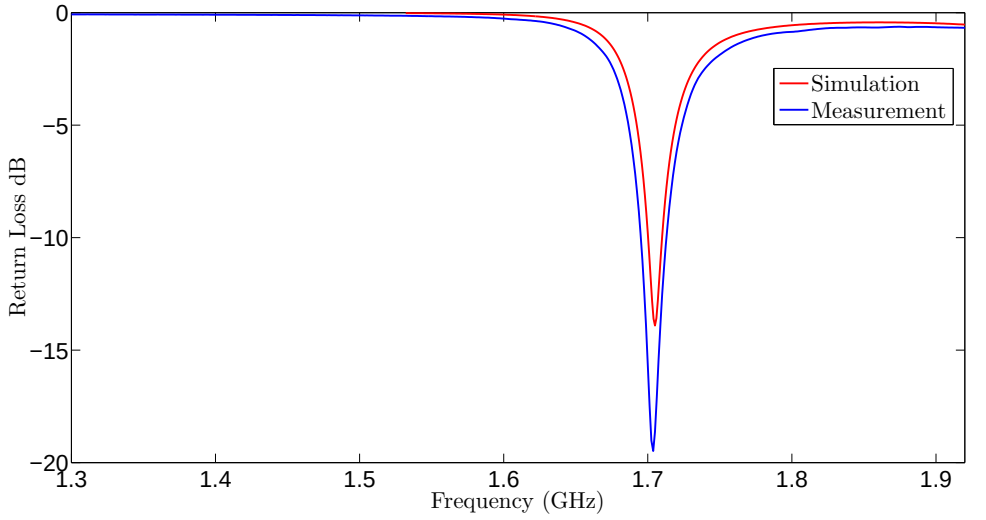

(b)

Figure 4.25: Simulations and measurements for Fig. 4.24: (a) Return loss (b) Input impedance

4.3.2 The length and angle of the probe

Similar to the rectangular cross-section cylinder, the impact of the probe's geometry is of interest for the circular cross-section cavity. The impact of the probe's geometry is investigated in the CBS antenna with the ferrite configuration illustrated in Fig. 4.21.

Probe angle

To investigate the impact of the angle of a triangular probe, the procedure outlined in Fig. 4.11 is used. Simulations show that a more acceptable impedance match is achieved for smaller angles; i.e., wire type of probe is the best geometry.

Probe length

Based on the previous section, the wire probe is the best option to excite the CBS antenna of Fig. 4.21. Simulations should be performed to observe how the length of the probe influences the radiation characteristics. Changing the length of the probe indicates that it does not really change the gain of the antenna; however, it has a severe impact on the return loss. Starting from 2 cm and extending the length of probe up to 4 cm, showed that the optimum length is 3.2 cm, which is almost about 0.75 of the wavelength at the resonant frequency.

4.3.3 Tunable Bandwidth

Using the definition presented for bandwidth in section 4.2.3, the tunable bandwidth of the CBS shown in Fig. 4.21 is about 133 MHz, which is 10% broader than that of the geometry of Fig. 4.8. Fig. 4.26 illustrates how the resonant frequency changes when different magnetic fields are applied.

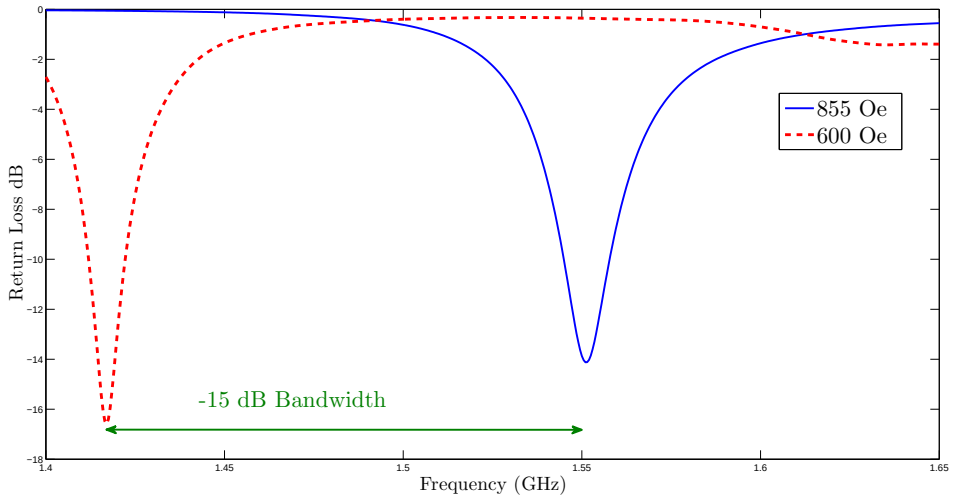

Figure 4.26: Tunable bandwidth of geometry of Fig. 4.21 for different magnetic fields

4.4 Circular Cross-Section Cavity; One-inch Height

The design procedure followed in this section for 1-inch height circular cross-section cavity is the same as the one for 2-inch height cavity in section 4.3. Therefore, instead of reviewing all of the details in this section, only some of the simulated geometries and corresponding results are presented.

Simulation of the CBS antenna of Fig. 3.5 without being loaded with ferrite material show that the antenna resonates at 6.5 GHz, with an S_{11} of -18 dB and gain of about 8 dBi at the mentioned frequency. The high gain is mainly because of the relative high resonant frequency. These results are illustrated in Fig. 4.27.

4.4.1 Ferrite Shaping and Positioning

Similar to section 4.3, the ferrite material is placed at different positions in the cavity. The gain and return loss for different geometries are obtained and finally the tunable bandwidth is determined. The ferrite material is placed on top of the probe at first.

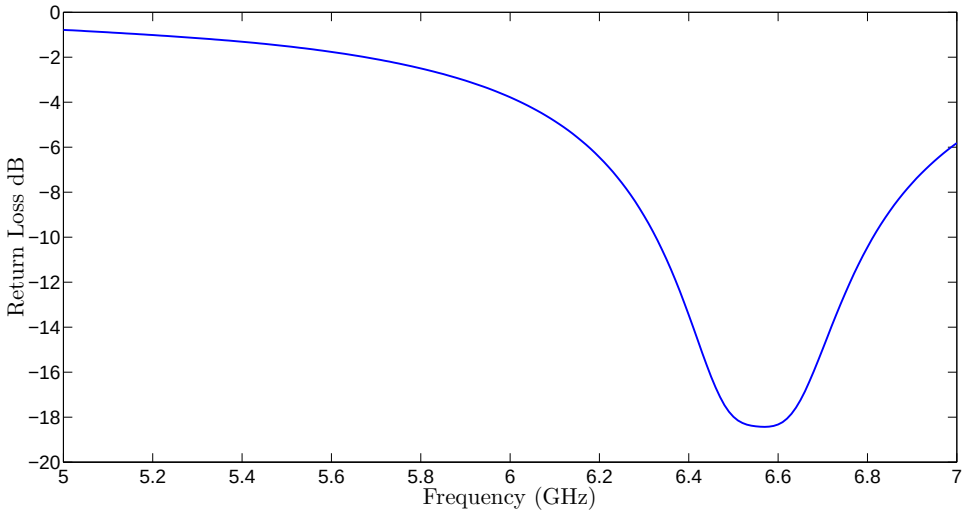

(a)

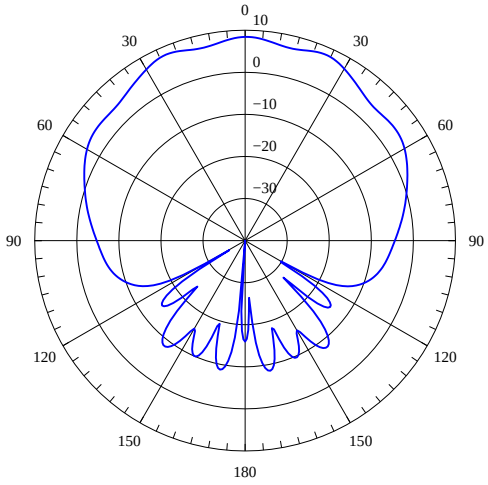

(b)

Figure 4.27: (a) Return loss of Fig. 4.19 (b) E-plane (YZ plane) pattern of the geometry of Fig. 4.19

Ferrite material on top of the probe

The radiation characteristics of Fig. 4.28 are shown in Fig. 4.29. As it can be seen in Fig. 4.29, new modes which are associated with ferrite material have appeared. Since the resonant frequency of the new mode is much lower (1.5 GHz) than that of the CBS antenna when it is not loaded with ferrite material, the gain has decreased substantially (-8 dBi); moreover, the impedance match is about -2 dB which is not acceptable.

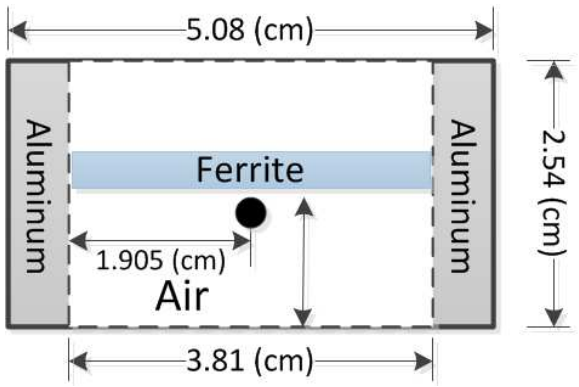

Figure 4.28: Circular cross-section cavity of height 1 inch with ferrite material on top of the probe

Ferrite material at the aperture

The second attempt is to examine the influence of an open aperture and relative placement of the ferrite material; therefore, the ferrite material is brought to the aperture and its center part is removed, as it was done in section 4.3.1. Based on the results obtained for the rectangular cross-section and circular cross-section (of height 2 inches) cavity, the gain is expected to increase. Simulations are verifying this, i.e., the gain improves to about 5 dBi. However, the S_{11} is still unacceptable. To achieve a better impedance match, larger fringing capacitances are required. Hence, more ferrite material is placed at the aperture and at the bottom of the cavity.

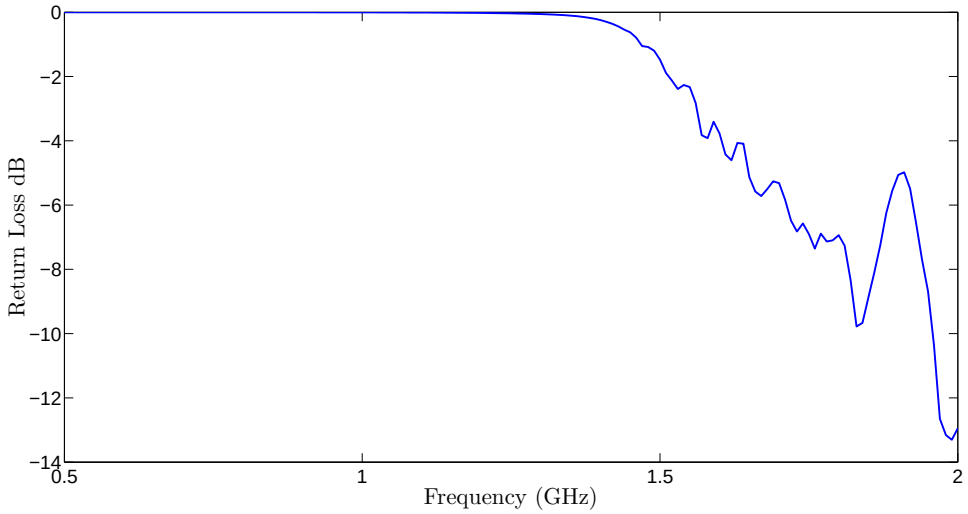

(a)

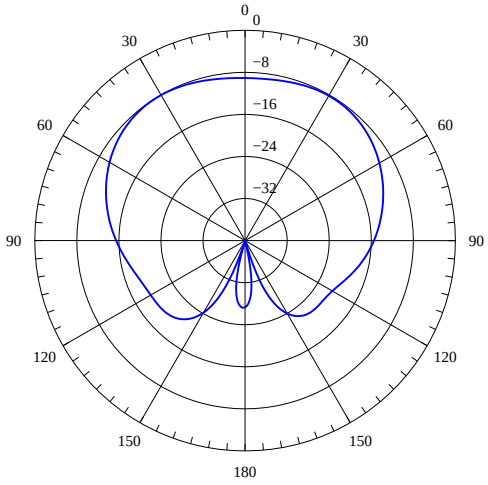

(b)

Figure 4.29: (a) Return loss of Fig. 4.28 (b) E-plane (YZ plane) pattern of the geometry of Fig. 4.28

Ferrite material at the aperture and on the bottom

Fig. 4.30 illustrates the configuration in which the cavity is loaded with ferrite material both at the aperture and on the bottom.

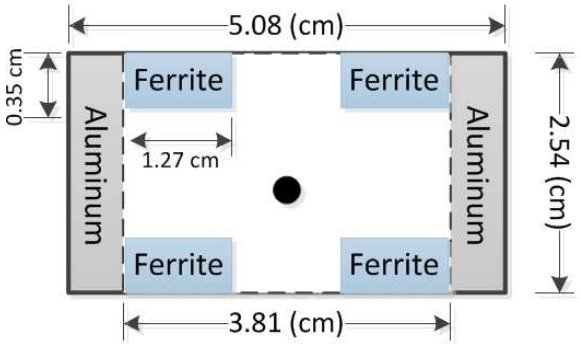

Figure 4.30: Circular cross-section cavity of height 1 inch with ferrite material at the aperture and on top of the probe

Simulations show that for the geometry of Fig. 4.30, it is impossible to achieve an impedance match below -15 dB and positive gain using the available ferrite. Applying an H_a of 570 Oe causes the antenna to resonate at 1.56 GHz with a gain of 1.06 dBi. The return loss at the mentioned frequency is about -10 dB. This is illustrated in Fig. 4.31.

To obtain a higher gain, it is necessary to apply a stronger magnetic field; however, the impedance match will be greater than -12 dB. If it is desired to improve the impedance match, a weaker DC magnetic field should be applied; however, the gain will decrease substantially (-5 dBi). The radiation characteristics of the antenna of Fig. 4.30 for H_a of 530 Oe is illustrated in Fig. 4.32. As it can be seen, the S_{11} is below -15 dB but the gain is -5 dBi.

Simulations show that for the circular cross-section cavity of height 1 inch, an impedance match of below -15 would be achieved at the expense of negative gain. Higher gains, on the other hand, are achievable at the expense of an impedance match

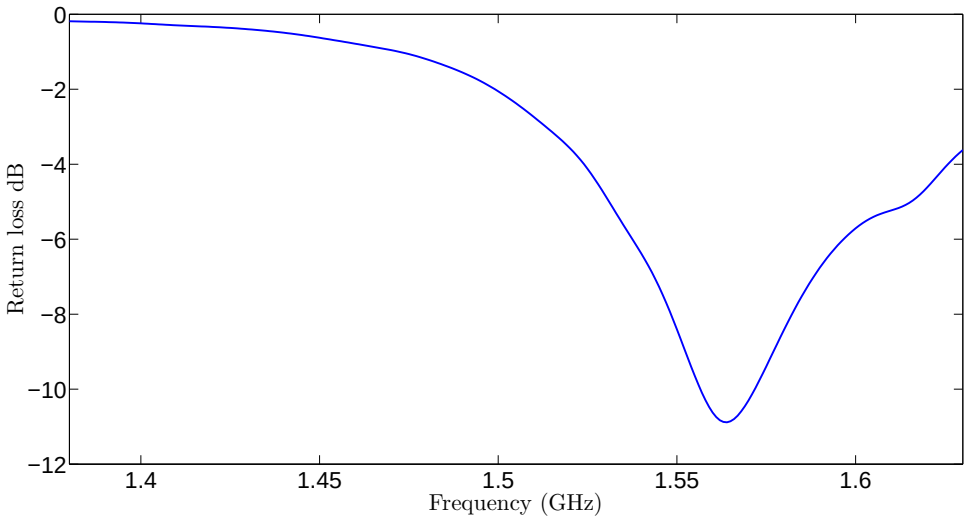

(a)

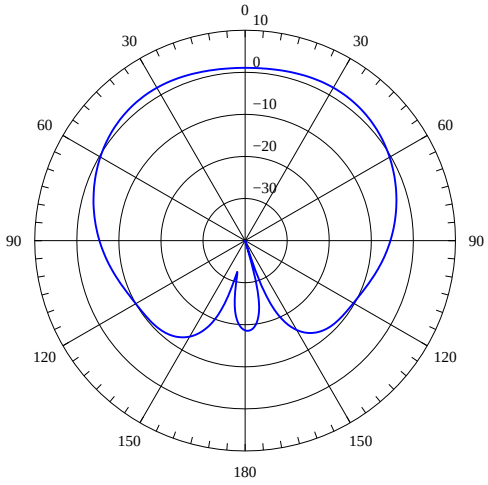

(b)

Figure 4.31: (a) Return loss of Fig. 4.30 (b) E-plane (YZ plane) pattern of the geometry of Fig. 4.30

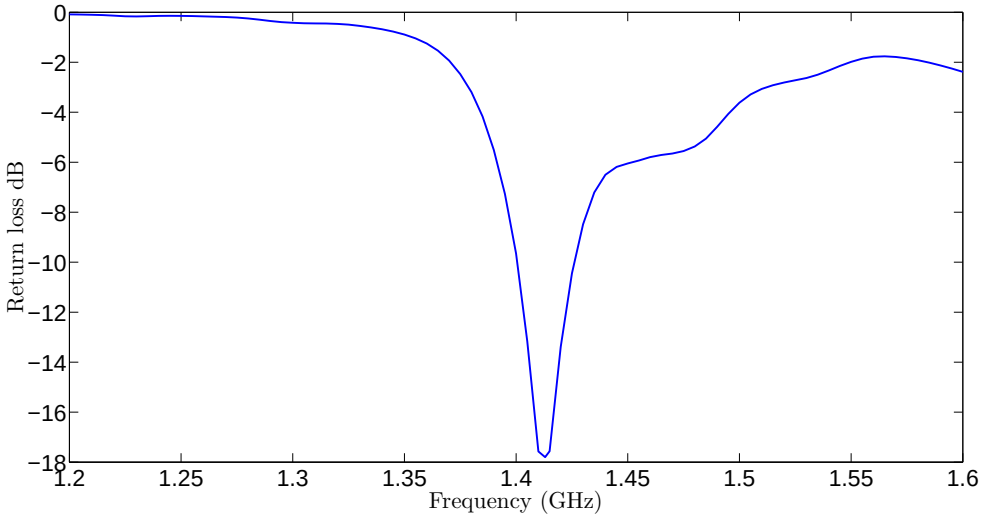

(a)

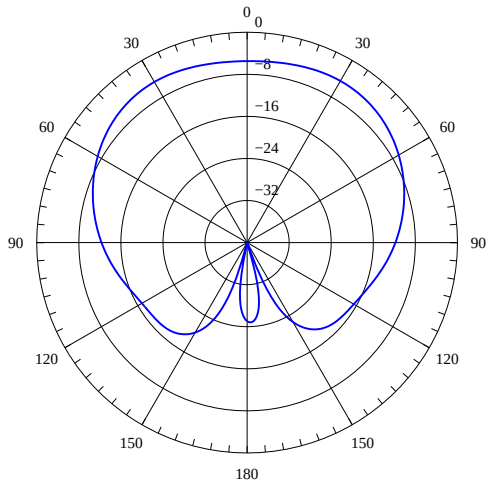

(b)

Figure 4.32: (a) Return loss of Fig. 4.30 (b) E-plane (YZ plane) pattern of the geometry of Fig. 4.30

above -15 dB. The geometry of the probe may be helpful to improve both the gain and the return loss.

4.4.2 The length and angle of the probe

Simulations show that, similar to the circular cross-section cavity of 2 inches, the wire type of probe is the best option to excite the 1-inch height circular cross-section cavity. Therefore the simulation results for different probe angles are not reported here. However, the resonant frequency for the configuration of the CBS antenna shown in Fig. 4.30 is different from that of Fig. 4.21. Hence, the impact of the length of the probe should be more carefully examined to see if it is possible to improve the figures-of-merit of the antenna.

To investigate the effects of probe length in the geometry of Fig. 4.30, the coil current was set to a value so that H_a was equal to 570 Oe. Fig. 4.33 illustrates the change of the resonant frequency and S_{11} versus the length of the probe. As it can be seen, an S_{11} below -15 dB can be achieved when the length is 2.265 cm. The gain; however, remains about 1 dBi and does not change significantly with the variation of the probe geometry.

4.4.3 Tunable Bandwidth

Using the definition presented in section 4.2.3, the -15 dB bandwidth of the circular cross-section cavity of height 1 inch with the ferrite configuration shown in Fig. 4.30 and the probe of length 2.265 cm is about 80 MHz.

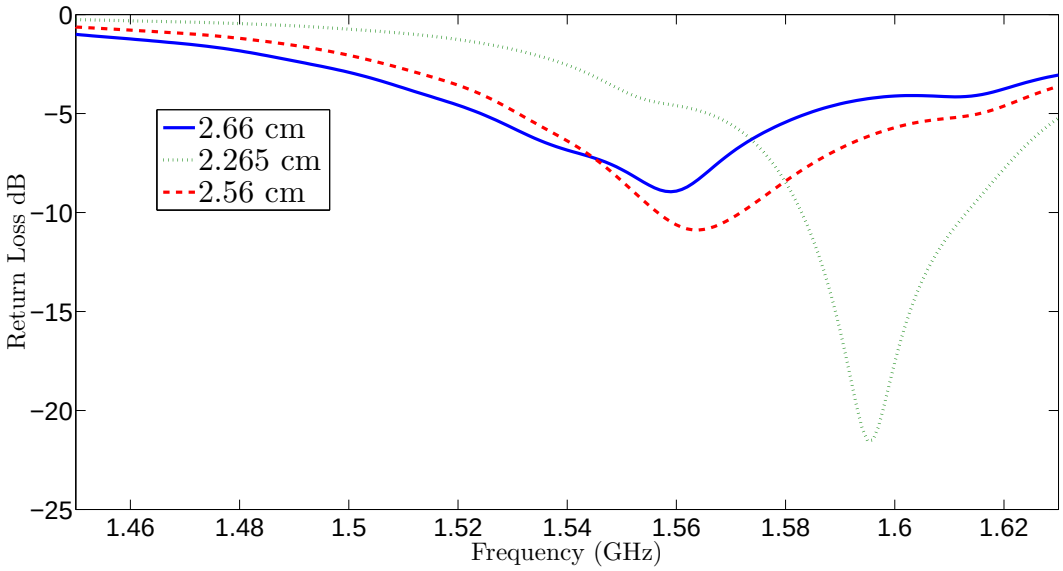

Figure 4.33: Return loss of the cavity configuration in Fig. 4.30 for different probe length

Chapter 5

Conclusions and Recommendations

5.1 Conclusions

In this thesis, different geometries of cavity-backed slot antenna (rectangular and circular cross-section cavities) were investigated. The main purpose of this study was to observe the impact of the shape and location of the ferrite material on the performance of the antenna. To obtain more accurate results, the applied magnetic field and magnetic field within the ferrite specimen were modeled based on the non-uniform approach. All of the simulations were performed in Ansys' Maxwell 3D and HFSS. The simulations were validated by comparing them to the results obtained from measurements. Eventually, the electric field distributions inside the cavity were examined to give physical interpretations of the impacts of the ferrite shaping and positioning on the antenna's performance.

The conclusions can be summarized as follows:

- Loading the cavity with ferrite material generally decreases the gain of the antenna due to the losses introduced by the ferrite; it may also impact the impedance match. The other influence is that new modes usually appear at lower frequencies, hence at the resonant frequency a lower gain would be obtained.

- The gain reduction, attributed to the ferrite's loss, can be alleviated by biasing the ferrite material so that it performs in its saturation zone. For the material used in this thesis (G-475), a magnetic field of about 3 Oe, internal to the ferrite, is sufficient for saturation [9].

- Introducing an open aperture, by removing parts of the lossy material, can also increase the gain for weak excitations; however, the tuning sensitivity of the

antenna decreases because of the lesser ferrite material inside the cavity. So a larger amount of ferrite material is need in the cavity.

- Applying a stronger magnetic field biases the ferrite sample more uniformly which excites a smaller number of propagation modes inside the cavity; hence, a better impedance match will be achieved. However, increasing the excitation field results in a higher resonant frequency because of a smaller permeability of the ferrite. On the other hand, biasing the ferrite material uniformly does not necessarily lead to -15 dB impedance match for all of the geometries. Such an impedance match can be achieved in certain geometries in which the ferrite samples are placed at strategic locations.

- For a higher gain, the electric field at the aperture must be more intense. A better impedance match is achieved in configurations with larger fringing capacitances; so electric fields must be stronger at the corners. This is the main reason why previous designs provided low gain and poor impedance match. In those designs, the intensity of the electric field at the aperture and corners was not strong sufficiently.

- Placing the ferrite material at the corners of the cavity results in larger fringing capacitances, which lead to a better impedance match. Therefore, a -15 dB S_{11} for lower magnetic field excitations and also wider tunable bandwidth will be achieved. For such geometry, the stronger fields occur close to the aperture, which eventually lead to higher gain.

Using these guidelines in design of the the CBS antenna leads to a higher gain (4 dBi for rectangular cross-section and 3 dBi for circular cross-section cavity), better impedance match and wider -15 dB bandwidth.

5.2 Future work

In this thesis, we attempted to optimize the radiation characteristics of the cavity-backed slot antenna; however, there is still more room for improvement. The major drawback of the CBS antenna is the narrow bandwidth. In this thesis, a -15 dB impedance bandwidth of 133 MHz was achieved; however, it would be a challenge to investigate if it is possible to widen the bandwidth by using other types of wideband probes. Spiral antennas, for instance, are broadband type of radiators. Thus, exciting the cavity with such a probe and examining if it has the same feature in a ferrite loaded environment can be a very rewarding challenge.

As it was shown in Chapter 4, the resonant frequency of the antenna increases as the intensity of the DC magnetic field increases. However, in the definition of the tunable bandwidth in this thesis, an upper limit for the intensity of the DC magnetic field was assumed. It would be of interest to define a tunable bandwidth with respect to the saturation of the ferrite material instead of magnetic field. Investigating the behaviour of the ferrite material and its impacts on the CBS antenna performance, in the presence of very strong magnetic field, can also be of interest.

REFERENCES

[1] V. G. Kononov, C. A. Balanis, and C. R. Birtcher, "Analysis, simulation and measurements of cbs antennas loaded with non-uniformly biased ferrite material," *IEEE Transactions on Antennas and Propagation*, vol. 60, no. 4, pp. 1717–1726, 2012.

[2] A. C. Polycarpou, C. A. Balanis, J. T. Aberle, and C. Birtcher, "Radiation and scattering from ferrite-tuned cavity-backed slot antennas: theory and experiment," *IEEE Transactions on Antennas and Propagation*, vol. 46, no. 9, pp. 1297–1306, 1998.

[3] M. N. Vouvakis, C. A. Balanis, C. R. Birtcher, and A. C. Polycarpou, "Ferrite-loaded cavity-backed antennas including nonuniform and nonlinear magnetization effects," *IEEE Transactions on Antennas and Propagation*, vol. 51, no. 5, pp. 1000–1010, 2003.

[4] S. Yoon, C. R. Birtcher, and C. A. Balanis, "Design of ferrite/dielectric-loaded cbs antennas," *IEEE Transactions on Antennas and Propagation*, vol. 53, no. 1, pp. 531–538, 2005.

[5] C. A. Balanis, *Advanced Engineering Electromagnetics*. (2nd edition) Wiley New York, 2012, vol. 205.

[6] D. Polder, "Viii. on the theory of ferromagnetic resonance," *Philosophical magazine*, vol. 40, no. 300, pp. 99–115, 1949.

[7] G. Tyras, "The permeability matrix for a ferrite medium magnetized at an arbitrary direction and its eigenvalues (correspondence)," *IRE Transactions on Microwave Theory and Techniques*, vol. 7, no. 1, pp. 176–177, 1959.

[8] D. M. Pozar, *Microwave Engineering*. John Wiley & Sons, 2009.

[9] *Microwave Magnetic and Dielectric Materials*. Trans-Tech 5520 Adamstown, MD 21710 USA, E-mail: transtech@alphaind.com, 2007.

[10] ANSYS, "Products, simulation technology, electromagnetics," Apr. 2012, http://www.ansys.com.